Optimization of Multimedia Progressive Transmission Over MIMO Channels

Seok-Ho Chang, *Member, IEEE*, Jihwan P. Choi, *Member, IEEE*, Pamela C. Cosman, *Fellow, IEEE*, and Laurence B. Milstein, *Fellow, IEEE*

***Abstract*—This paper studies the optimal transmission of multimedia progressive sources, which require unequal target error rates in their bitstream, over multiple-input–multiple-output (MIMO) channels. First, we derive the information outage probability expression of a space–time code for an arbitrarily given piecewise-linear diversity–multiplexing tradeoff (DMT) function and the conditions for the existence of a crossover point of the information outage probability curves of the space–time codes. We prove that as long as the crossover point of the outage probabilities exists, as spectral efficiency increases, the crossover point in the signal-to-noise ratio (SNR) monotonically increases, whereas that of the outage probability monotonically decreases. This analysis can be applied to any space–time code, receiver, and propagation channel with a given DMT function. As a specific example, we analyze the two-layer diagonal Bell Labs space–time architecture (D-BLAST) with a group zero-forcing receiver, the vertical BLAST (V-BLAST) with a minimum mean-square error receiver, and orthogonal space–time block codes (OSTBCs), and prove the monotonic behavior of the crossover point for those codes. Based on that, with respect to D-BLAST, V-BLAST, and OSTBC, we derive a method for the optimal space–time coding of a sequence that contains numerous progressive packets. We show that by employing the optimization method rather than exhaustive search, the computational complexity involved with optimal space–time coding can be exponentially reduced without losing any peak SNR performance.**

***Index Terms*—Diagonal Bell Labs space–time architecture (D-BLAST), diversity–multiplexing tradeoff (DMT), group zero-forcing receiver, information outage probability, minimum mean-square error (MMSE) receiver, multimedia progressive sources, multiple-input multiple-output (MIMO) systems, orthogonal space–time block codes (OSTBCs), vertical Bell Labs space–time architecture (V-BLAST).**

Manuscript received July 31, 2014; revised December 16, 2014; accepted January 17, 2015. Date of publication March 12, 2015; date of current version March 10, 2016. This research was supported by the Basic Science Research Program through the National Research Foundation of Korea (NRF) funded by the Ministry of Education (2013R1A1A2065143), by the US National Science Foundation under grant CCF-1160832, by DGIST through the MIREBraiN program, and by the research fund of Dankook University (BK21 Plus) in 2014. The review of this paper was coordinated by Dr. N.-D. Đào. *(Corresponding author: Jihwan P. Choi.)*

S.-H. Chang is with the Department of Computer Science and Engineering, Dankook University, Yongin 448-701, Korea (e-mail: seokho@dankook.ac.kr).

J. P. Choi is with the Department of Information and Communications Engineering, Daegu Gyeongbuk Institute of Science and Technology, Daegu 711-873, Korea (e-mail: jhchoi@dgist.ac.kr).

P. C. Cosman and L. B. Milstein are with the Department of Electrical and Computer Engineering, University of California, San Diego, La Jolla, CA 92093-0407 USA (e-mail: pcosman@ucsd.edu; milstein@ece.ucsd.edu).

Color versions of one or more of the figures in this paper are available online at http://ieeexplore.ieee.org.

Digital Object Identifier 10.1109/TVT.2015.2412655

I. Introduction

In recent years, there has been significant demand for the transmission of multimedia services over wireless channels, and this has motivated intense research for cross-layer optimization design [1]–[3], which is particularly important for mobile radio channels that exhibit time-variant channel-quality fluctuations. Embedded image or scalable video coders [4]–[7] employ a progressive manner of transmission such that as more bits are successfully received, the source can be reconstructed with better quality. Such progressive coders are usually sensitive to channel impairments.

The use of multiple-input multiple-output (MIMO) technology is an important advance in wireless communications. A large gain in transmission data rates can be provided by spatial multiplexing [8], [9], and link reliability can be significantly improved by transmit diversity schemes [10], [11]. In this paper, we study the optimal design of such a MIMO system for the transmission of multimedia progressive sources. Progressive sources have the key feature that they have steadily decreasing importance for bits later in the stream, which makes unequal target error rates and/or transmission data rates in the stream very useful. Hence, when progressive sources are transmitted over MIMO channels, and each block of the stream can be encoded with a different space–time code, the tradeoff between the space–time codes under consideration should be clarified in terms of their target error rates and transmission data rates.

In [12], spatial multiplexing and orthogonal space–time block codes (OSTBCs) were compared from the viewpoint of information outage probability and uncoded bit error rate, and the way the crossover point of the error probability curves behave in the high signal-to-noise ratio (SNR) regime was analyzed. In [12], it was proven that for spatial multiplexing and OSTBC, as the data rate increases, the crossover point in error probability monotonically decreases, whereas that in the SNR monotonically increases. Then, the analysis was exploited for the optimal space–time coding of progressive sources, i.e., it was used to optimally assign spatial multiplexing or OSTBC to each block of the stream to be transmitted over independent and identically distributed (i.i.d.) Rayleigh fading channels. The numerical results showed that, using the optimization method in [12], the computational complexity involved with the optimization is exponentially simplified, without losing any peak signal-to-noise ratio (PSNR) performance.

In [12], only the vertical Bell Labs space–time architecture (V-BLAST) with a zero-forcing receiver and OSTBC in i.i.d. Rayleigh fading channels is analyzed. In this paper, with different technical approaches from those used in [12], we extend the work in [12] to other space–time codes and receivers and show the monotonic behavior of their crossover points, which is valid in propagation channels such as spatially correlated Rayleigh and Rician fading channels, in addition to i.i.d. Rayleigh fading channels. To do so, we exploit the diversity–multiplexing tradeoff (DMT) [13], which has become a standard tool in the characterization of the performance of space–time codes at high SNR and in the large spectral efficiency regime. First, we derive the information outage probability expression of the space–time code for an arbitrarily given piecewise-linear DMT function, and then analyze the crossover point of the outage probability curves of the codes with any given DMT functions. These results are presented in Section II.

The analysis in Section II can be applied to any type of space–time code and receiver with a known piecewise-linear DMT function. As a specific example, in Section III, we analyze the crossover point for the two-layer diagonal Bell Labs space–time architecture (D-BLAST) with a group zero-forcing receiver [14] and V-BLAST with a minimum mean-square error (MMSE) receiver, in addition to OSTBC. Note that space–time block codes, which can yield the benefits of both spatial diversity and multiplexing, have been studied in [15]–[20]. Spatial multiplexing, such as V-BLAST, does not exploit transmit diversity; however, it does achieve high data rates; OSTBC, which decouples the streams at the receiver, extracts full diversity at the cost of a limited spatial multiplexing rate. However, if a larger receiver complexity is available, it is possible to relax the condition of decoupling the streams at the receiver and increase the data rates while still providing transmit diversity [21]. Codes based on that principle are linear dispersion codes [15], [16]. The Golden code [17], which is a class of codes known as perfect space–time block codes [18], is constructed from cyclic division algebra [21] and achieves the optimal DMT characteristics. Another algebraic code built from cyclic division algebra was proposed in [19], which also achieves the optimal DMT characteristics. Other constructions based on cyclic division algebra can be found in [20]. Those kinds of space–time block codes in general require high receiver complexity to achieve the optimal DMT characteristics. On the other hand, in Section III, we consider low-complexity space–time block codes with linear receivers that retain suboptimal DMT characteristics. Note that novel wireless communication systems are targeting very large spectral efficiencies, because of hot spots and picocell arrangements [22]. For such systems, employing high data rates and a large number of antennas, the use of low-complexity space–time codes and linear receivers may be required, due to complexity and power consumption issues.

In Section IV, based on the results in Section III, we optimize the space–time coding of progressive sources, which require unequal target error rates in their bitstream, with respect to D-BLAST, V-BLAST, and OSTBC. Section V presents numerical results, and we conclude this paper in Section VI.

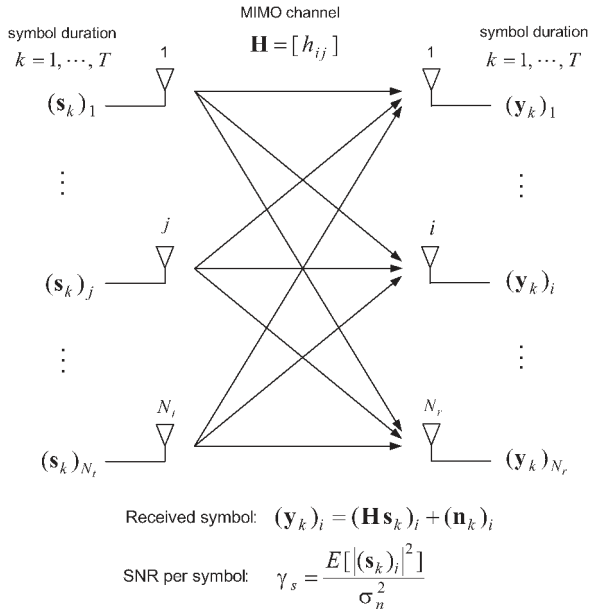

Fig. 1. System model with N_t transmit and N_r receive antennas. A space–time codeword $\mathbf{S}=[\mathbf{s}_1\cdots\mathbf{s}_T]$ of size $N_t\times T$ is transmitted over T symbol durations.

II. Crossover Point Analysis of the Outage Probability Curves for Given Diversity–Multiplexing Tradeoff Functions

First, we present the system model. Consider a narrowband MIMO system with N_t transmit and N_r receive antennas communicating over a frequency flat-fading channel, as shown in Fig. 1. A space–time codeword, $\mathbf{S}=[\mathbf{s}_1\cdots\mathbf{s}_T]$ of size $N_t\times T$ is transmitted over T symbol durations through N_t transmit antennas. The baseband equivalent model of the MIMO system, at the kth time symbol duration ($k=1,\ldots,T$), is given by

$$\mathbf{y}_k=\mathbf{H}\mathbf{s}_k+\mathbf{n}_k \tag{1}$$

where $\mathbf{s}_k$ is the $N_t\times 1$ transmitted signal vector, $\mathbf{y}_k$ is the $N_r\times 1$ received signal vector, and $\mathbf{n}_k$ is an $N_r\times 1$ noise vector at the output of a matched filter. The variable $\mathbf{n}_k$ is zero-mean complex additive white Gaussian noise with $\mathcal{E}[\mathbf{n}_k\mathbf{n}_l^H]=\sigma_n^2\mathbf{I}_{N_r}\delta(k-l)$, where $(\cdot)^H$ denotes Hermitian operation. In (1), $\mathbf{H}$ denotes the $N_r\times N_t$ channel matrix, whose entry h_{ij} represents the complex channel gain between the jth transmit antenna and the ith receive antenna, and the entries are i.i.d. complex Gaussian random variables with zero mean and unit variance. It is assumed that $\mathbf{H}$ is random but constant over T symbol durations (quasi-static Rayleigh i.i.d. fading). Let γ_s denote SNR per symbol, which is defined as $\gamma_s:=\mathcal{E}[|(\mathbf{s}_k)_i|^2]/\sigma_n^2$, where $(\mathbf{s}_k)_i$ is the ith component of $\mathbf{s}_k$ ($i=1,\ldots,N_t$). We assume that $\mathbf{H}$ is known at the receiver but not known at the transmitter.

Next, we derive the outage probability expression of the space–time code for any given piecewise-linear DMT function. Let r and d denote the multiplexing and diversity gains defined in [13], respectively. That is

$$R=\lim_{\gamma_s\to\infty}\frac{R(\gamma_s)}{\log\gamma_s} \tag{2}$$

$$D=-\lim_{\gamma_s\to\infty}\frac{\log P_{\text{out}}(\gamma_s)}{\log\gamma_s} \tag{3}$$

where $R(\gamma_s)$ is the spectral efficiency (bits/s/Hz), and $P_{\text{out}}(\gamma_s)$ is the outage probability. In this paper, all the logarithms are assumed to be taken with respect to base 2. By L'Hopital's rule, (2) can be expressed as

$$r = \lim_{\gamma_s \to \infty} \frac{\partial R(\gamma_s)/\partial \gamma_s}{\partial \log \gamma_s / \partial \gamma_s} = \lim_{\gamma_s \to \infty} \ln 2 \cdot \gamma_s \frac{\partial R(\gamma_s)}{\partial \gamma_s}. \quad (4)$$

Eq. (4) can be rewritten as

$$\lim_{\gamma_s \to \infty} \frac{\partial R(\gamma_s)}{\partial \gamma_s} = \lim_{\gamma_s \to \infty} \frac{r}{\ln 2} \gamma_s^{-1}. \quad (5)$$

By integrating both sides of (5), we have

$$\lim_{\gamma_s \to \infty} R(\gamma_s) = \lim_{\gamma_s \to \infty} r \log \gamma_s + c_r \quad (6)$$

where c_r is an arbitrary real constant. Let $k_r = 2^{c_r} > 0$. Then, as $\gamma_s \to \infty$ (i.e., high SNR), $R(\gamma_s)$ can be expressed as

$$R(\gamma_s) = \log(k_r \gamma_s^r). \quad (7)$$

In a similar way, from L'Hopital's rule, (3) can be rewritten as

$$d = -\lim_{\gamma_s \to \infty} \frac{\partial P_{\text{out}}(\gamma_s)/\partial \gamma_s}{\partial \log \gamma_s / \partial \gamma_s} = -\lim_{\gamma_s \to \infty} \ln 2 \cdot \gamma_s \frac{\partial \log P_{\text{out}}(\gamma_s)}{\partial \gamma_s}. \quad (8)$$

From (8), we have

$$\lim_{\gamma_s \to \infty} \log P_{\text{out}}(\gamma_s) = \lim_{\gamma_s \to \infty} -d \log \gamma_s + c_d \quad (9)$$

where c_d is a real arbitrary constant. As $\gamma_s \to \infty$, $P_{\text{out}}(\gamma_s)$ can be expressed as

$$P_{\text{out}}(\gamma_s) = k_d \gamma_s^{-d} \quad (10)$$

where $k_d = 2^{c_d} > 0$.

Consider a space–time code whose DMT characteristic function, which is defined in [13], is given by

$$d^\dagger(r) = v - ur, \quad \text{for } \alpha \le r \le \beta (\alpha > 0) \quad (11)$$

where $d^\dagger(r) \ge 0$, and $u \ge 0$ and $v \ge 0$ are real constants. Let $P_{\text{out}}^\dagger(\gamma_s)$ denote the outage probability for the space–time code whose DMT is given by (11). From (10) and (11), as $\gamma_s \to \infty$, $P_{\text{out}}^\dagger(\gamma_s)$ can be expressed as

$$P_{\text{out}}^\dagger(\gamma_s) = k_d \gamma_s^{-d^\dagger(r)} = k_d \frac{\gamma_s^{ur}}{\gamma_s^v}. \quad (12)$$

Eq. (7) can be rewritten as

$$\gamma_s^r = \frac{2^{R(\gamma_s)}}{k_r} > 1 \quad (13)$$

where the inequality follows from $\gamma_s \gg 1$ (i.e., high SNR) and $r > 0$. Substituting (13) into (12), as $\gamma_s \to \infty$, $P_{\text{out}}^\dagger(\gamma_s)$ can be rewritten as

$$P_{\text{out}}^\dagger(\gamma_s) = k_d \left(\frac{2^{R(\gamma_s)}}{k_r} \right)^u \frac{1}{\gamma_s^v} \quad (14)$$

for $(2^{R(\gamma_s)}/k_r)^{1/\beta} \le \gamma_s \le (2^{R(\gamma_s)}/k_r)^{1/\alpha}$. The range of γ_s is derived as follows. Since $r > 0$, (13) can be rewritten as $\gamma_s = (2^{R(\gamma_s)}/k_r)^{1/r}$. Thus, from the inequality in (13) and $\alpha \le r \le \beta$ in (11), we have the range of γ_s in (14). We focus on the situation that the spectral efficiency, i.e., $R(\gamma_s)$, does not change as γ_s increases. That is, $R(\gamma_s)$ is fixed regardless of SNR. The motivation for this will be described in Section IV. Thus, from here onward, we denote the spectral efficiency, i.e., $R(\gamma_s)$, simply by R. In the following sections, for given piecewise-linear DMT functions of the space–time codes, we analyze the crossover points of their outage probability curves.

A. Case When There Exists a Crossover in the DMT Functions

We first analyze the case where there exists a crossover in the DMT characteristic functions. Consider two space–time codes that have linear DMT characteristics as follows:

$$d_1(r) = v_1 - u_1 r \quad \text{and} \quad d_2(r) = v_2 - u_2 r \quad \text{for} \quad \alpha \le r \le \beta (\alpha > 0) \quad (15)$$

where

$$u_i > 0 \quad \text{and} \quad v_i > 0 \quad (i = 1, 2) \quad (16)$$

$$v_1 - u_1 \alpha < v_2 - u_2 \alpha \quad (17)$$

$$v_1 - u_1 \beta > v_2 - u_2 \beta. \quad (18)$$

That is, there exists a crossover in $\alpha < r < \beta$ for the two DMT functions. Let $P_{\text{out},1}(\gamma_s)$ and $P_{\text{out},2}(\gamma_s)$ denote the outage probabilities of the space–time codes whose DMT functions are given by $d_1(r)$ and $d_2(r)$, respectively. Then, from (14), as $\gamma_s \to \infty$, we have

$$P_{\text{out,i}}(\gamma_s) = k_d \left(\frac{2^R}{k_r} \right)^{u_i} \frac{1}{\gamma_s^{v_i}} (i = 1, 2) \quad (19)$$

for $(2^R/k_r)^{1/\beta} \le \gamma_s \le (2^R/k_r)^{1/\alpha}$. From (19), for a given spectral efficiency, i.e., R, we find the SNR, i.e., γ_s^*, for which $P_{\text{out},1}(\gamma_s)$ and $P_{\text{out},2}(\gamma_s)$ are identical. It can be readily shown that, for $v_1 \ne v_2$, γ_s^* is given by

$$\gamma_s^* = \left(\frac{2^R}{k_r} \right)^{\frac{u_2 - u_1}{v_2 - v_1}}. \quad (20)$$

In the following, we will show that γ_s^* exists within the range of SNR in (19) and that $v_1 \ne v_2$, or, more precisely, $v_2 > v_1$ for (20).

i) From (17) and (18), we obtain $(\beta - \alpha)u_2 > (\beta - \alpha)u_1$, or, equivalently, $u_2 > u_1$. By multiplying (17) and (18) by β and α, respectively, it can be shown that $v_2 > v_1$.
ii) From $u_2 > u_1$ and $v_2 > v_1$, (17) and (18) can be rewritten as $1/\alpha > (u_2 - u_1)/(v_2 - v_1)$ and $1/\beta < (u_2 - u_1)/$

$(v_2 - v_1)$, respectively. From this and the inequality in (13), we have

$$\left(\frac{2^R}{k_r}\right)^{\frac{1}{\beta}} \leq \gamma_s^* \leq \left(\frac{2^R}{k_r}\right)^{\frac{1}{\alpha}}. \tag{21}$$

Furthermore, from $u_2 > u_1$ and $v_2 > v_1$, it follows that γ_s^*, given by (20), is a strictly increasing function in R, as long as $k_r > 0$ is. In other words, as the spectral efficiency increases, the crossover point of the outage probability curves in SNR monotonically increases.

If we substitute γ_s^*, given by (20), into (19), it can be shown that the corresponding outage probability, i.e., P_{out}^*, is given by

$$P_{\text{out}}^* = k_d \left(\frac{2^R}{k_r}\right)^{\frac{u_1 v_2 - u_2 v_1}{v_2 - v_1}}. \tag{22}$$

We will prove that P_{out}^* is a strictly decreasing function in R: From $u_2 > u_1$ and $v_2 > v_1$, (18) can be rewritten as $\beta > (v_2 - v_1)/(u_2 - u_1)$. From $d_2(\beta) = v_2 - u_2\beta \geq 0$, which is assumed in (15), and $u_2 > 0$, given by (16), it is seen that $\beta \leq v_2/u_2$. Thus, we have $(v_2 - v_1)/(u_2 - u_1) < v_2/u_2$. From this, $u_2 > 0$, and $u_2 > u_1$, it can be shown that $u_2 v_1 > u_1 v_2$. In addition, from $v_2 > v_1$, we have

$$\frac{u_1 v_2 - u_2 v_1}{v_2 - v_1} < 0. \tag{23}$$

Eqs. (22) and (23) show that P_{out}^* is a strictly decreasing function in R, regardless of what the constants $k_d > 0$ and $k_r > 0$ are. That is, as the spectral efficiency increases, the crossover point in the outage probability monotonically decreases.

Moreover, from (19) and $v_2 > v_1$, it can be shown that

$$\begin{aligned} &P_{\text{out},1}(\gamma_s) < P_{\text{out},2}(\gamma_s) \quad \text{for} \quad \left(\frac{2^R}{k_r}\right)^{\frac{1}{\beta}} \leq \gamma_s < \gamma_s^* \\ &P_{\text{out},1}(\gamma_s) > P_{\text{out},2}(\gamma_s) \quad \text{for} \quad \gamma_s^* < \gamma_s \leq \left(\frac{2^R}{k_r}\right)^{\frac{1}{\alpha}}. \end{aligned} \tag{24}$$

Let $P_{\text{out,f}}^*$ and $\gamma_{s,f}^*$ denote the crossover point when a spectral efficiency $R = R_f$ is used, and let $P_{\text{out,g}}^*$ and $\gamma_{s,g}^*$ denote the crossover point when a spectral efficiency $R = R_g$ is employed. Suppose that $R_f < R_g$. Since γ_s^* and P_{out}^* are strictly increasing and decreasing functions in R, respectively, we have

$$\gamma_{s,f}^* < \gamma_{s,g}^* \quad \text{and} \quad P_{\text{out,f}}^* > P_{\text{out,g}}^* \quad \text{for} \quad R_f < R_g. \tag{25}$$

Based on (24) and (25), the outage probabilities of the two space–time codes, for the same given spectral efficiency, are qualitatively shown in Fig. 2. Suppose that a target outage probability, i.e., $P_{\text{out,T}}$, is smaller than $P_{\text{out,f}}^*$ but greater than $P_{\text{out,g}}^*$. Then, in Fig. 2, it is seen that, for a spectral efficiency R_f, the space–time code with the DMT of $d_2(r)$ given by (15) is preferable to that with the DMT of $d_1(r)$. For a spectral efficiency R_g, however, the latter is preferable to the former. Note that the analyses in this section are valid for any $k_d > 0$ and $k_r > 0$.

B. Case When the DMT Functions Coincide Only at the Lowest Multiplexing Gain

We next analyze the case when the DMT functions coincide only at the smallest multiplexing gain in the range $\alpha \leq r \leq \beta$. Consider two space–time codes that have linear DMT characteristics given by (15) with

$$u_i > 0 \quad \text{and} \quad v_i > 0 \quad (i = 1, 2) \tag{26}$$

$$v_1 - u_1\alpha = v_2 - u_2\alpha \tag{27}$$

$$v_1 - u_1\beta < v_2 - u_2\beta. \tag{28}$$

In the following, we will show that $u_1 > u_2$ and $v_1 > v_2$.

i) Assume that $u_1 < u_2$. From this assumption, (27), and (28), it is seen that $\alpha = (v_2 - v_1)/(u_2 - u_1)$ and $\beta < (v_2 - v_1)/(u_2 - u_1)$. From these, we have $\beta < \alpha$, which is inconsistent with $\alpha \leq \beta$ given by (15).
ii) Next, we assume that $u_1 = u_2$. Then, from (27) and (28), $v_1 = v_2$ and $v_1 < v_2$ are derived, which is a contradiction.
iii) Finally, we assume that $u_1 > u_2$. Then, from (27) and $\alpha > 0$ [given by (15)], $v_1 > v_2$ is derived.

From $v_1 > v_2$ and (27), we have $1/\alpha = (u_2 - u_1)/(v_2 - v_1)$. Thus, γ_s^*, given by (20), exists in the range of SNR, given by (19), in a manner such that

$$\left(\frac{2^R}{k_r}\right)^{\frac{1}{\beta}} \leq \gamma_s \leq \left(\frac{2^R}{k_r}\right)^{\frac{1}{\alpha}} (= \gamma_s^*). \tag{29}$$

Moreover, from $u_1 > u_2$ and $v_1 > v_2$, it is seen that γ_s^* is a strictly increasing function in R, for any $k_r > 0$. In other words, as the spectral efficiency increases, the crossover point in SNR monotonically increases.

In the following, we will prove that P_{out}^*, given by (22), is a strictly decreasing function in R. From $u_1 > u_2$ and $v_1 > v_2$, (28) can be expressed as $\beta > (v_2 - v_1)/(u_2 - u_1)$. From $d_2(\beta) = v_2 - u_2\beta \geq 0$ in (15) and $u_2 > 0$ in (26), we have $\beta \leq v_2/u_2$. Thus, we have $(v_2 - v_1)/(u_2 - u_1) < v_2/u_2$. From this, $u_2 > 0$, and $u_1 > u_2$, it can be shown that $u_2 v_1 < u_1 v_2$. From this and $v_1 > v_2$, it follows that

$$\frac{u_1 v_2 - u_2 v_1}{v_2 - v_1} < 0. \tag{30}$$

From (22) and (30), it is seen that P_{out}^* is a strictly decreasing function in R, for any $k_d > 0$ and $k_r > 0$. That is, as the spectral efficiency increases, the crossover point in the outage probability monotonically decreases.

Furthermore, from (19) and $v_1 > v_2$, it can be shown that

$$P_{\text{out},1}(\gamma_s) > P_{\text{out},2}(\gamma_s) \quad \text{for} \quad \left(\frac{2^R}{k_r}\right)^{\frac{1}{\beta}} \leq \gamma_s < \left(\frac{2^R}{k_r}\right)^{\frac{1}{\alpha}}. \tag{31}$$

From (31), it is seen that, except at the highest SNR, $\gamma_s = (2^R/k_r)^{1/\alpha}$, the space–time code with the DMT given by $d_2(r)$ is always preferable to the space–time code with the DMT given by $d_1(r)$, for any spectral efficiency R and target outage probability $P_{\text{out,T}}$. Note that this differs from the result in Section II-A, which is stated below (25). However, as described

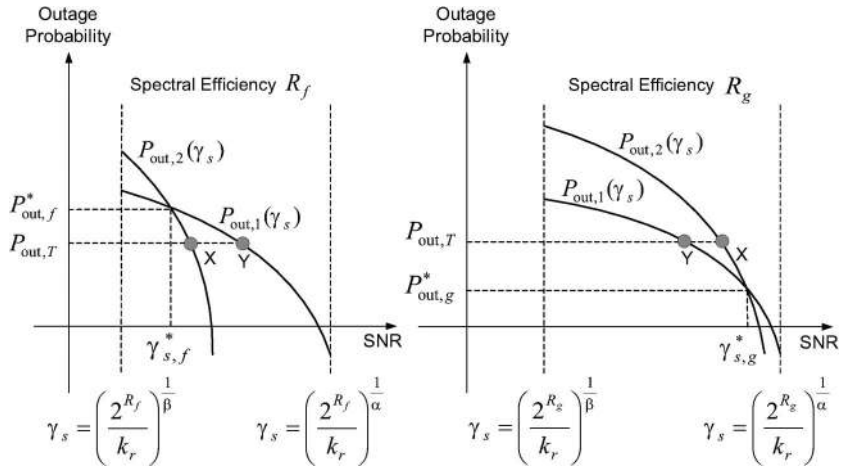

Fig. 2. Outage probabilities of the two space–time codes for the same given spectral efficiency. For $R_f < R_g$, the outage probabilities have the following properties: 1) $\gamma^*_{s,f} < \gamma^*_{s,g}$; 2) $P^*_{\text{out,f}} > P^*_{\text{out,g}}$; 3) $P_{\text{out},1}(\gamma_s) < P_{\text{out},2}(\gamma_s)$ for $(2^{R_f}/k_r)^{1/\beta} \le \gamma_s < \gamma^*_{s,f}$ or $(2^{R_g}/k_r)^{1/\beta} \le \gamma_s < \gamma^*_{s,g}$; $P_{\text{out},1}(\gamma_s) > P_{\text{out},2}(\gamma_s)$ for $\gamma^*_{s,f} < \gamma_s \le (2^{R_f}/k_r)^{1/\alpha}$ or $\gamma^*_{s,g} < \gamma_s \le (2^{R_g}/k_r)^{1/\alpha}$.

below (29) and (30), the crossover point, γ^*_s, and P^*_{out} retain the same properties as those in Section II-A. That is

$$\gamma^*_{s,f} < \gamma^*_{s,g} \quad \text{and} \quad P^*_{\text{out,f}} > P^*_{\text{out,g}} \quad \text{for} \quad R_f < R_g. \tag{32}$$

This will be used for the analysis in Section III.

C. Case When the DMT Functions Coincide Only at the Highest Multiplexing Gain

Here, we analyze the case when the DMT functions coincide only at the largest multiplexing gain in the range $\alpha \le r \le \beta$. Consider two space–time codes that have linear DMT characteristics given by (15) with

$$u_1 \ge 0, u_2 > 0, v_1 \ge 0, \quad \text{and} \quad v_2 > 0 \tag{33}$$

$$v_1 - u_1\alpha < v_2 - u_2\alpha \tag{34}$$

$$v_1 - u_1\beta = v_2 - u_2\beta. \tag{35}$$

In a similar manner to Section II-B, it can be shown that γ^*_s, given by (20), exists in the range of SNR, given by (19), in a way such that

$$\left(\frac{2^R}{k_r}\right)^{\frac{1}{\beta}} (= \gamma^*_s) \le \gamma_s \le \left(\frac{2^R}{k_r}\right)^{\frac{1}{\alpha}}. \tag{36}$$

Furthermore, it can be shown that

$$P_{\text{out},1}(\gamma_s) > P_{\text{out},2}(\gamma_s) \quad \text{for} \quad \left(\frac{2^R}{k_r}\right)^{\frac{1}{\beta}} < \gamma_s \le \left(\frac{2^R}{k_r}\right)^{\frac{1}{\alpha}}. \tag{37}$$

That is, except at the lowest SNR, the space–time code with the DMT given by $d_2(r)$ is preferable to that with the DMT given by $d_1(r)$, for any R and $P_{\text{out,T}}$. This is different from the result in Section II-A.

D. Case When the DMT Functions Differ for Any Multiplexing Gain

We take into account the case when the DMT functions are different over the entire range $\alpha \le r \le \beta$. Consider two space–time codes that have linear DMT characteristics given by (15), with

$$u_1 \ge 0, u_2 > 0, v_1 \ge 0, \quad \text{and} \quad v_2 > 0 \tag{38}$$

$$v_1 - u_1\alpha < v_2 - u_2\alpha \tag{39}$$

$$v_1 - u_1\beta < v_2 - u_2\beta. \tag{40}$$

It can be shown that for all u_i and v_i $(i = 1, 2)$ satisfying (38)–(40), we have $\{u_1 > u_2, v_1 > v_2\}$, $\{u_1 > u_2, v_1 = v_2\}$, and $\{\forall u_1, \forall u_2, v_1 < v_2\}$. For each set, we will show that γ^*_s, given by (20), does not exist in the range of SNR given by (19).

i) $\{u_1 > u_2, v_1 > v_2\}$: From $\alpha > 0$ in (15) and (39), we have $1/\alpha = (u_2 - u_1)/(v_2 - v_1)$, i.e., $(2^R/k_r)^{1/\alpha} < \gamma^*_s$.
ii) $\{u_1 > u_2, v_1 = v_2\}$: From (19), it is seen that there exists no γ^*_s for which $P_{\text{out},1}(\gamma_s)$ and $P_{\text{out},2}(\gamma_s)$ are the same.
iii) $\{\forall u_1, \forall u_2, v_1 < v_2\}$: From $\beta > 0$ in (15) and (40), it follows that $(u_2 - u_1)/(v_2 - v_1) < 1/\beta$, i.e., $\gamma^*_s < (2^R/k_r)^{1/\beta}$.

Next, for each set above, we will show that

$$P_{\text{out},1}(\gamma_s) > P_{\text{out},2}(\gamma_s) \quad \text{for} \quad \left(\frac{2^R}{k_r}\right)^{\frac{1}{\beta}} \le \gamma_s \le \left(\frac{2^R}{k_r}\right)^{\frac{1}{\alpha}}. \tag{41}$$

i) $\{u_1 > u_2, v_1 > v_2\}$: From (19), it is seen that $P_{\text{out},1}(\gamma_s)/P_{\text{out},2}(\gamma_s)$ is a strictly decreasing function in γ_s. We have already shown that $(2^R/k_r)^{1/\alpha} < \gamma^*_s$; thus, (41) is valid.
ii) $\{u_1 > u_2, v_1 = v_2\}$: From (19) and the inequality in (13), it follows that (41) holds.
iii) $\{\forall u_1, \forall u_2, v_1 < v_2\}$: From (19), $P_{\text{out},1}(\gamma_s)/P_{\text{out},2}(\gamma_s)$ is a strictly increasing function in γ_s. Since $\gamma^*_s < (2^R/k_r)^{1/\beta}$, (41) is valid.

From (41), it is seen that the space–time code with the DMT given by $d_2(r)$ is preferable to that with the DMT given by $d_1(r)$, for any R and $P_{\text{out,T}}$.

E. Case When the DMT Functions Coincide

Finally, we consider the case when the DMT functions coincide over the entire range $\alpha \le r \le \beta$. Consider two space–time codes that have linear DMT characteristics given by (15), with

$$u_1 = u_2 \ge 0 \quad \text{and} \quad v_1 = v_2 \ge 0. \tag{42}$$

From (19) and (42), we have

$$P_{\text{out},1}(\gamma_s) = P_{\text{out},2}(\gamma_s) \quad \text{for} \quad \left(\frac{2^R}{k_r}\right)^{\frac{1}{\beta}} \le \gamma_s \le \left(\frac{2^R}{k_r}\right)^{\frac{1}{\alpha}}. \tag{43}$$

That is, the two space–time codes are equally preferable.

III. Crossover Point Analysis of the Outage Probability Curves for D-BLAST, V-BLAST, and OSTBC

Here, based on the analysis in Section II, we analyze the behavior of the crossover point of the outage probability curves for specific space–time codes. As an example, we take three space–time codes into consideration: two-layer D-BLAST with a group zero-forcing receiver [14], V-BLAST with an MMSE receiver, and OSTBC with a decorrelator. Group decoding (group detection) is a recent decoding method studied in [23]–[28]. By dividing all symbols into multiple groups, the group zero-forcing decoding is performed in two steps, i.e., nulling the interference from all the other groups and then maximum-likelihood decoding the symbols in the current group. It can be regarded as a compromise between zero forcing and maximum-likelihood decoding. From here onward, unless stated otherwise, D-BLAST, V-BLAST, and OSTBC are assumed to be with those specific receivers. The DMT characteristics of D-BLAST, V-BLAST, and OSTBC, which are denoted by $d_D(r)$, $d_V(r)$, and $d_O(r)$, respectively, are given by [14], [21], [29]

$$d_D(r) = \begin{cases} N_r N_t - N_t + 1 - \frac{1}{2}N_r(N_t+1)r \\ \quad \text{for} \quad 0 \le r \le \frac{2}{N_t+1} \\ (N_r-1)N_t - \frac{1}{2}(N_r-1)(N_t+1)r \\ \quad \text{for} \quad \frac{2}{N_t+1} \le r \le \frac{2N_t}{N_t+1} \\ 0, \quad \text{for} \quad \frac{2}{N_t+1} \le r < \infty \end{cases} \tag{44}$$

$$d_V(r) = \begin{cases} N_r - N_t + 1 - \frac{1}{N_t}(N_r - N_t + 1)r \\ \quad \text{for} \quad 0 \le r \le N_t \\ 0, \quad \text{for} \quad N_t \le r < \infty \end{cases} \tag{45}$$

$$d_O(r) = \begin{cases} N_r N_t - \frac{1}{r_s}N_r N_t r, \quad \text{for} \quad 0 \le r \le r_s \\ 0, \quad \text{for} \quad r_s \le r < \infty \end{cases} \tag{46}$$

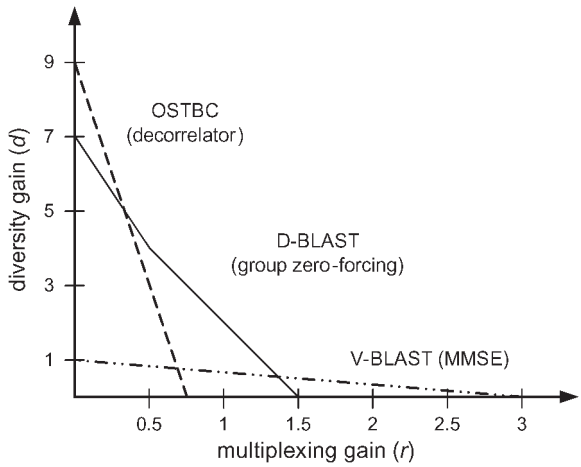

Fig. 3. DMT characteristics of D-BLAST with a group zero-forcing receiver, V-BLAST with an MMSE receiver, and OSTBC with decorrelator in 3×3 MIMO systems. Note that for D-BLAST, two linear curves are joined at $r = 0.5$ and $d = 4$.

where r_s is the spatial multiplexing rate of the OSTBC, which is defined as the ratio of the number of symbols packed within a space–time codeword to the time duration of a space–time codeword. For $N_t = 2$, the Alamouti scheme achieves $r_s = 1$. On the other hand, $r_s = 3/4$ is the maximum achievable rate for $N_t = 3$ or 4 in the complex OSTBC, and $r_s = 1/2$ is the maximum rate for $N_t > 4$ [30]. As an example, the DMT characteristics for 3×3 MIMO systems are shown in Fig. 3. Here, to compare the given space–time codes, it is assumed that $N_r \ge N_t \ge 2$.

A. Two-Layer D-BLAST With a Group Zero-Forcing Receiver and V-BLAST With an MMSE Receiver

We first analyze D-BLAST and V-BLAST. The range of multiplexing gain, which is given by (44) and (45), can be divided into $0 < r \le 2/(N_t+1)$, $2/(N_t+1) \le r \le 2N_t/(N_t+1)$, $2N_t/(N_t+1) \le r \le N_t$, and $N_t \le r < \infty$, such that the DMT functions of both D-BLAST and V-BLAST are linear over each range. Based on the results in Section II, for each of the ranges, we analyze the crossover point of the outage probability curves of D-BLAST and V-BLAST. The proof of the following analysis is given in Appendix A.

i) $0 < r \le 2/(N_t+1)$: For this range, the result in Section II-D, given by (41), holds for $(2^R/k_r)^{(N_t+1)/2} \le \gamma_s < \infty$ (i.e., D-BLAST is preferable to V-BLAST).

ii) $2/(N_t+1) \le r \le 2N_t/(N_t+1)$: For this case, the result in Section II-A, given by (24) and (25), holds for $(2^R/k_r)^{(N_t+1)/2N_t} \le \gamma_s \le (2^R/k_r)^{(N_t+1)/2}$ (i.e., there exists a crossover point, γ_s^* and P_{out}^*, in the outage probability curves; V-BLAST is preferable to D-BLAST for $\gamma_s < \gamma_s^*$, and D-BLAST is preferable otherwise; the crossover point, γ_s^* and P_{out}^*, exhibits a monotonic behavior as spectral efficiency increases).

iii) $2N_t/(N_t+1) \le r \le N_t$: The result in Section II-C, given by (37), holds for $(2^R/k_r)^{1/N_t} \le \gamma_s \le (2^R/k_r)^{(N_t+1)/2N_t}$ (i.e., V-BLAST is preferable to D-BLAST, except at $\gamma_s = (2^R/k_r)^{1/N_t}$).

iv) $N_t \le r < \infty$: For this range, the result in Section II-E, given by (43), holds for $1 < \gamma_s \le (2^R/k_r)^{1/N_t}$ (i.e., D-BLAST and V-BLAST are equally preferable).

Let $P_{\text{out,D}}(\gamma_s)$ and $P_{\text{out,V}}(\gamma_s)$ denote the outage probabilities of D-BLAST and V-BLAST, respectively. The results of i), ii), iii), and iv) can be summarized as follows:

$$\begin{aligned} &P_{\text{out,D}}(\gamma_s) = P_{\text{out,V}}(\gamma_s) \quad \text{for} \quad 1 < \gamma_s \le \left(\frac{2^R}{k_r}\right)^{\frac{1}{N_t}} \\ &P_{\text{out,D}}(\gamma_s) > P_{\text{out,V}}(\gamma_s) \quad \text{for} \quad \left(\frac{2^R}{k_r}\right)^{\frac{1}{N_t}} < \gamma_s < \gamma_s^* \\ &P_{\text{out,D}}(\gamma_s) < P_{\text{out,V}}(\gamma_s) \quad \text{for} \quad \gamma_s^* < \gamma_s < \infty \end{aligned} \tag{47}$$

where γ_s^* exists in the range of $(2^R/k_r)^{(N_t+1)/2N_t} < \gamma_s < (2^R/k_r)^{(N_t+1)/2}$, and it exhibits monotonic behavior, as given by (25), i.e.,

$$\gamma_{s,f}^* < \gamma_{s,g}^* \quad \text{and} \quad P_{\text{out,f}}^* > P_{\text{out,g}}^* \quad \text{for} \quad R_f < R_g. \tag{48}$$

Suppose that a target outage probability, i.e., $P_{\text{out,T}}$, is smaller than $P_{\text{out,f}}^*$ but greater than $P_{\text{out,g}}^*$. Then, from (47) and (48), it is seen that D-BLAST is preferable to V-BLAST for a spectral efficiency R_f, but V-BLAST is preferable for R_g (see Fig. 2).

B. Two-Layer D-BLAST With a Group Zero-Forcing Receiver and OSTBC With a Decorrelator

We next analyze D-BLAST and OSTBC. The range of multiplexing gains, given by (44) and (46), can be divided into $0 < r \le 2/(N_t+1)$, $2/(N_t+1) \le r \le r_s$, $r_s \le r \le 2N_t/(N_t+1)$, and $2N_t/(N_t+1) \le r < \infty$ such that the DMT functions of both D-BLAST and OSTBC are linear for each range. We first take into account the case of $N_t \ge 3$. The proof of the following analysis is presented in Appendix B.

Case 1: $N_r \ge N_t \ge 3$

i) $0 < r \le 2/(N_t+1)$: For this range, the result in Section II-A, which is given by (24) and (25), holds for $(2^R/k_r)^{(N_t+1)/2} \le \gamma_s < \infty$ (i.e., there exists a crossover point, γ_s^*, and P_{out}^*, in the outage probability curves; D-BLAST is preferable for $\gamma_s < \gamma_s^*$, and OSTBC is preferable otherwise; the crossover point, γ_s^*, and P_{out}^* exhibit a monotonic behavior as spectral efficiency increases).
ii) $2/(N_t+1) \le r \le r_s$: For this case, the result in Section II-D, which is given by (41), holds for $(2^R/k_r)^{1/r_s} \le \gamma_s \le (2^R/k_r)^{(N_t+1)/2}$ (i.e., D-BLAST is preferable to OSTBC).
iii) $r_s \le r \le 2N_t/(N_t+1)$: The result in Section II-C, which is given by (37), holds for $(2^R/k_r)^{(N_t+1)/2N_t} \le \gamma_s \le (2^R/k_r)^{1/r_s}$ (i.e., D-BLAST is preferable to OSTBC except at $\gamma_s = (2^R/k_r)^{(N_t+1)/2N_t}$).
iv) $2N_t/(N_t+1) \le r < \infty$: The result in Section II-E, which is given by (43), holds for $1 < \gamma_s \le (2^R/k_r)^{(N_t+1)/2N_t}$ (i.e., D-BLAST and OSTBC are equally preferable).

Let $P_{out,O}(\gamma_s)$ denote the outage probability of OSTBC. The results of i), ii), iii), and iv) are summarized in the following:

$$\begin{aligned} &P_{\text{out,D}}(\gamma_s) = P_{\text{out,O}}(\gamma_s) \quad \text{for} \quad 1 < \gamma_s \le \left(\frac{2^R}{k_r}\right)^{\frac{N_t+1}{2N_t}} \\ &P_{\text{out,D}}(\gamma_s) < P_{\text{out,O}}(\gamma_s) \quad \text{for} \quad \left(\frac{2^R}{k_r}\right)^{\frac{N_t+1}{2N_t}} < \gamma_s < \gamma_s^* \\ &P_{\text{out,D}}(\gamma_s) > P_{\text{out,O}}(\gamma_s) \quad \text{for} \quad \gamma_s^* < \gamma_s < \infty \end{aligned} \tag{49}$$

where γ_s^* exists in the range of $(2^R/k_r)^{(N_t+1)/2} < \gamma_s < \infty$, and it exhibits a monotonic behavior, as given by (25), i.e.,

$$\gamma_{s,f}^* < \gamma_{s,g}^* \quad \text{and} \quad P_{\text{out,f}}^* > P_{\text{out,g}}^* \quad \text{for} \quad R_f < R_g. \tag{50}$$

Case 2: $N_t = 2$ and $N_r \ge 4$

We have the same results as those of i), ii), iii), and iv) of Case 1.

Case 3: $N_t = 2$ and $N_r = 3$

i) $0 < r \le 2/(N_t+1)$: For this range, the result in Section II-C, which is given by (37), holds for $(2^R/k_r)^{(N_t+1)/2} \le \gamma_s < \infty$ (i.e., OSTBC is preferable to D-BLAST, except at $\gamma_s = (2^R/k_r)^{(N_t+1)/2}$).
ii) $2/(N_t+1) \le r \le 1$: The result in Section II-B, which is given by (31) and (32), holds for $2^R/k_r \le \gamma_s \le (2^R/k_r)^{(N_t+1)/2}$ (i.e., D-BLAST, is preferable to OSTBC, except at $\gamma_s = (2^R/k_r)^{(N_t+1)/2}$; the crossover point, γ_s^* and P_{out}^*, exhibits a monotonic behavior as spectral efficiency increases).
iii) $1 \le r \le 2N_t/(N_t+1)$: This is the same result as that of iii) of Case 1.
iv) $2N_t/(N_t+1) \le r < \infty$: This is the same result as that of iv) of Case 1.

The results of i), ii), iii), and iv) can also be summarized as given by (49); however, the crossover point is exactly $\gamma_s^* = (2^R/k_r)^{(N_t+1)/2}$; it also exhibits a monotonic behavior, as given by (32), or, equivalently, (50).

Case 4: $N_t = N_r = 2$

i) $0 < r \le 2/(N_t+1)$: For this range, the result in Section II-D, which is given by (41), holds for $(2^R/k_r)^{(N_t+1)/2} \le \gamma_s < \infty$ (i.e., OSTBC is preferable to D-BLAST).
ii) $2/(N_t+1) \le r \le 1$: The result in Section II-A, which is given by (24) and (25), holds for $2^R/k_r \le \gamma_s \le (2^R/k_r)^{(N_t+1)/2}$ (i.e., there exists a crossover point γ_s^* and P_{out}^*, in the outage probability curves; D-BLAST is preferable for $\gamma_s < \gamma_s^*$, and OSTBC is preferable otherwise; the crossover point γ_s^* and P_{out}^*, exhibits a monotonic behavior as spectral efficiency increases).
iii) $1 \le r \le 2N_t/(N_t+1)$: This is the same result as that of iii) of Case 1.
iv) $2N_t/(N_t+1) \le r < \infty$: This is the same result as that of iv) of Case 1.

The results of i), ii), iii), and iv) can also be summarized as given by (49); however, γ_s^* exists in the range of $2^R/k_r <$

$\gamma_s < (2^R/k_r)^{(N_t+1)/2}$; it also exhibits a monotonic behavior, as given by (25) or, equivalently, (50).

Suppose that a target outage probability, i.e., $P_{\text{out,T}}$, is smaller than $P^*_{\text{out,f}}$ but greater than $P^*_{\text{out,g}}$. Then, for all the Cases 1, 2, 3, and 4, from (49) and (50), it is seen that OSTBC is preferable to D-BLAST for a spectral efficiency R_f, but D-BLAST is preferable for R_g (see Fig. 2).

C. V-BLAST With an MMSE Receiver and OSTBC With a Decorrelator

In a similar manner, it can be readily shown that, for V-BLAST and OSTBC, we have

$$P_{\text{out,V}}(\gamma_s) = P_{\text{out,O}}(\gamma_s), \quad \text{for} \quad 1 < \gamma_s \le \left(\frac{2^R}{k_r}\right)^{\frac{1}{N_t}}$$

$$P_{\text{out,V}}(\gamma_s) < P_{\text{out,O}}(\gamma_s), \quad \text{for} \quad \left(\frac{2^R}{k_r}\right)^{\frac{1}{N_t}} < \gamma_s < \gamma_s^*$$

$$P_{\text{out,V}}(\gamma_s) > P_{\text{out,O}}(\gamma_s), \quad \text{for} \quad \gamma_s^* < \gamma_s < \infty \tag{51}$$

where γ_s^* exists in the range of $(2^R/k_r)^{1/r_s} < \gamma_s^* < \infty$, and it exhibits a monotonic behavior, as given by (25), i.e.,

$$\gamma^*_{s,f} < \gamma^*_{s,g} \text{ and } P^*_{\text{out,f}} > P^*_{\text{out,g}} \text{ for } R_f < R_g. \tag{52}$$

Suppose that a target outage probability, i.e., $P_{\text{out,T}}$, is smaller than $P^*_{\text{out,f}}$ but greater than $P^*_{\text{out,g}}$. Then, from (51) and (62), it is seen that OSTBC is preferable to V-BLAST for a spectral efficiency R_f, but V-BLAST is preferable for R_g. Note that the results are consistent with those of the analyses for V-BLAST with a zero-forcing receiver and OSTBC that are presented in [12]. The results are not contrary to our expectation, since the DMT functions of an MMSE receiver and a zero-forcing receiver for V-BLAST are exactly the same.

IV. Optimal Space–Time Coding of a Progressive Bitstream

We exploit the analysis in Section III to address the optimization of progressive transmission in MIMO systems. In the following, we summarize the properties of progressive sources, as described in [12, Sec. III], from the viewpoint of their target error rates and transmission data rates.

Progressive encoders produce encoded data with gradual differences of importance in their bitstreams. Suppose that the bitstream from a progressive source encoder is transformed into a sequence of N_P packets, as shown in Fig. 4. Each of those packets can be encoded with different transmission data rates, as well as different space–time codes, to yield the best end-to-end performance as measured by the expected distortion of the source. The error probability of an earlier packet needs to be less than or equal to that of a later packet, due to the decreasing importance in the progressive bitstream. Thus, given the same transmission power, the earlier packet requires a transmission data rate that is less than or equal to that of the later packet.

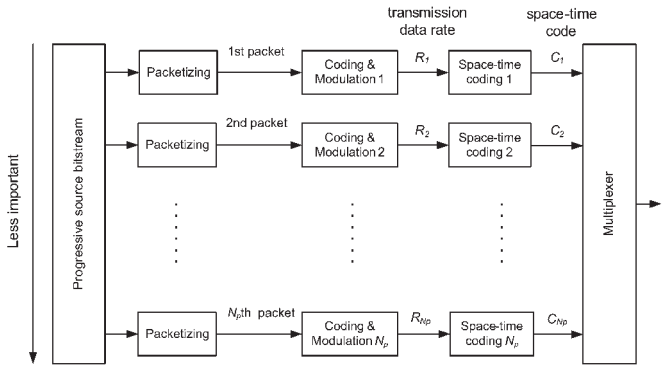

Fig. 4. Progressive source transmission system. R_i and C_i denote the transmission data rate and the space–time code assigned to the ith packet, respectively ($1 \le i \le N_P$).

Let N_R denote the number of candidate transmission data rates employed by a system. The number of possible assignments of N_R data rates to N_P packets would exponentially grow as N_P increases. Furthermore, in a MIMO system, if each packet can be encoded with different space–time codes (e.g., D-BLAST, V-BLAST, or OSTBC), the assignment of space–time codes, as well as data rates to N_P packets, yields a more complicated optimization problem. Note that each source, such as an image, has its inherent rate-distortion characteristic, from which the performance of the expected distortion is computed. Hence, for example, when a series of images is transmitted, the said optimization should be addressed in a real-time manner, considering which specific image (i.e., rate-distortion characteristic) is transmitted in the current time slot. To address this matter, for a single-input–single-output system, there have been some studies about the optimal assignment of data rates to a sequence of progressive packets [31]–[33].

For a MIMO system, we exploit the results in the previous section to optimize the assignment of space–time codes to progressive packets. First, we focus on D-BLAST and V-BLAST. Suppose that we can employ either D-BLAST or V-BLAST for each progressive packet and that the kth packet in a sequence of N_P packets is encoded with V-BLAST. Then, our analysis tells us that the $k+1$st, $k+2$nd, …, N_Pth packets also should be encoded with V-BLAST rather than with D-BLAST. This is because in Section III, we have proven that when V-BLAST is preferable for a packet with a data rate (i.e., spectral efficiency) of R_f, a packet with a data rate of R_g ($> R_f$) should also be encoded with V-BLAST, as long as the target error rate of the latter is the same as or higher than that of the former (see Fig. 2). That is, in a sequence of N_P progressive packets, the last i consecutive packets should be encoded with V-BLAST, and the other $N_P - i$ packets are encoded with D-BLAST ($0 \le i \le N_P$).

Next, suppose that either D-BLAST or OSTBC can be employed for each packet and that the kth packet is encoded with OSTBC. Then, the first, second, …, $k-1$st packets also should be encoded with OSTBC. This is because in Section III, we have shown that when OSTBC is preferable for a packet with a rate of R_g, a packet with a rate of $R_f (< R_g)$ also should be encoded with OSTBC, as long as the target error rate of the

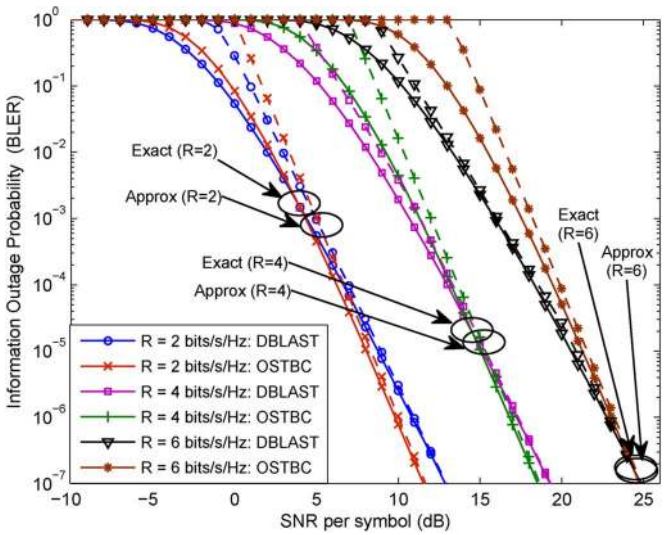

Fig. 5. Exact and high-SNR approximate outage probabilities of D-BLAST and OSTBC for 2×3 MIMO systems in i.i.d. Rayleigh fading channels. Solid curves denote the exact outage probabilities, and dashed curves denote the high-SNR approximate outage probabilities. The exact and approximate crossover points are marked with circles.

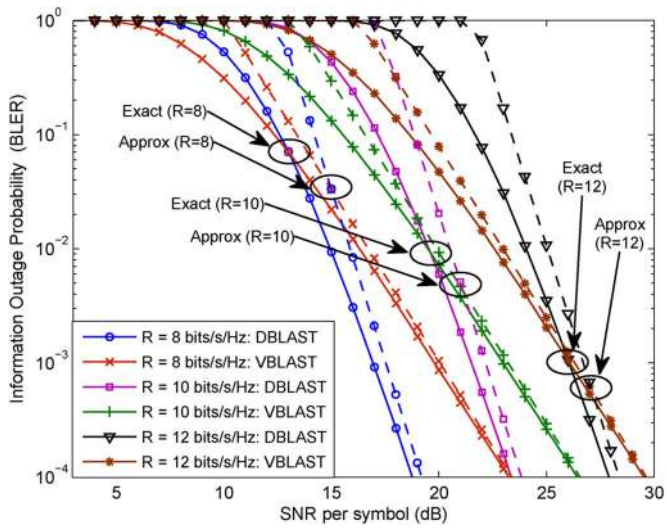

Fig. 6. Exact and high-SNR approximate outage probabilities of D-BLAST and V-BLAST for 2×4 MIMO systems in i.i.d. Rayleigh fading channels. Solid curves denote the exact outage probabilities, and dashed curves denote the high-SNR approximate outage probabilities. The exact and approximate crossover points are marked with circles.

latter is the same as or lower than that of the former. Hence, the earliest i consecutive packets should be encoded with OSTBC, whereas the other $N_P - i$ packets are encoded with D-BLAST ($0 \leq i \leq N_P$).

From the previous statements, the optimization strategy regarding D-BLAST, V-BLAST, and OSTBC can be derived as follows: Suppose that the system can employ D-BLAST, V-BLAST, or OSTBC for each progressive packet. Then, the earliest i consecutive packets should be encoded with OSTBC, the last j consecutive packets should be encoded with V-BLAST, and the remaining $N_P - i - j$ packets are encoded with D-BLAST ($0 \leq i, j \leq N_P$ and $0 \leq i + j \leq N_P$).

As a result, it can be shown that the number of possible assignments of the three space–time codes to a sequence of N_P packets is reduced from 3^{N_P} to $\binom{N_P+1}{2}$. The computational complexity involved with the optimization can be exponentially simplified.

V. Numerical Evaluation and Discussion

First, we numerically evaluate the outage probabilities of D-BLAST, V-BLAST, and OSTBC for various spectral efficiencies and numbers of transmit and receive antennas. The results for 2×3 and 2×4 MIMO systems are shown in Figs. 5 and 6, respectively,[1] where solid curves denote the exact outage probabilities, and dashed curves denote the high-SNR approximate outage probabilities that are derived from (11), (14), and (44)–(46). Note that the analyses in Sections II and III are valid for any $k_d > 0$ and $k_r > 0$ in the high-SNR approximate outage probabilities. In Figs. 5 and 6, we set the constant k_d in (14) to unity such that, at low SNR, we have $P_{\mathrm{out,D}}(\gamma_s) = P_{\mathrm{out,V}}(\gamma_s) = P_{\mathrm{out,O}}(\gamma_s) = k_d = 1$, where the third equality follows from (11), (14), and the last lines of (44)–(46) [i.e., $u = v = 0$ are substituted into (14)]. Another constant k_r is chosen such that, at high SNR, the SNR gap between the high-SNR approximate outage probability and the exact SNR approximate outage probability is small. In Figs. 5 and 6, the exact outage probabilities are obtained by numerically evaluating [12, Eq. (20)], [14, Eq. (15)], and [22, Eqs. (6) and (9)] for OSTBC, D-BLAST, and V-BLAST, respectively. Note that in those equations, mutual information is normalized by the time duration of a space–time codeword [i.e., T as defined above (1)] for the computation of the outage probabilities. Figs. 5 and 6 show that as spectral efficiency increases, the exact crossover points as well as the approximate crossover points behave in a manner predicted by the analysis as given by (48) and (50).

In Fig. 7, the exact outage probabilities of D-BLAST, V-BLAST, and OSTBC are shown together, for 2×2 MIMO systems with several spectral efficiencies. If we focus on an outage probability of 10^{-3}, D-BLAST shows the best performance for the spectral efficiency of 12 bits/s/Hz, whereas OSTBC exhibits the best for 8 and 10 bits/s/Hz. Note that this preference is a function of spectral efficiency as well as the target outage probability of an application. For example, if the target is $2 \cdot 10^{-1}$, V-BLAST is the best for 12 bits/s/Hz, whereas D-BLAST is the best for 8 and 10 bits/s/Hz. Fig. 8 shows the exact outage probabilities for 4×4 MIMO systems. It is seen that as spectral efficiency increases, the crossover points behave as predicted by (48) and (50), similar to the case of 2×2 MIMO systems. Note that, compared with 2×2 MIMO systems, OSTBC performs well only at very high SNR. This is, in part, because the multiplexing rate is only 3/4 in the complex OSTBC for $N_t = 3$ or 4 [30], unlike the case of $N_t = 2$, where the Alamouti scheme achieves a multiplexing rate of 1.

In the following, we compare the optimal space–time coding and the suboptimal space–time coding for progressive

[1]For other spectral efficiencies and numbers of antennas, the corresponding crossover points exhibit the same behavior; thus, they are not depicted here.

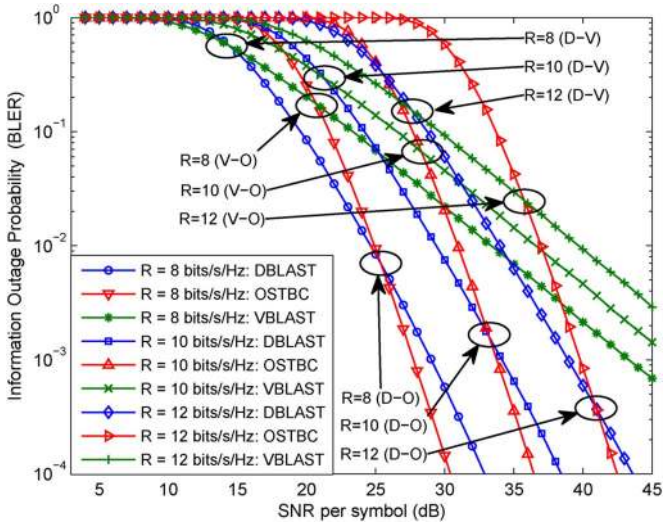

Fig. 7. Exact outage probabilities of D-BLAST, V-BLAST, and OSTBC for 2×2 MIMO systems in i.i.d. Rayleigh fading channels. The crossover points are marked with circles, where D-O, D-V, and V-O denote the crossover points for D-BLAST/OSTBC, D-BLAST/V-BLAST, and V-BLAST/OSTBC, respectively.

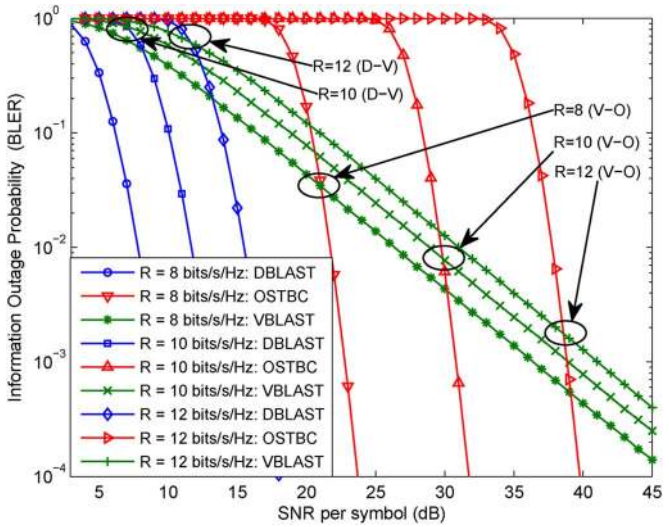

Fig. 8. Exact outage probabilities of D-BLAST, V-BLAST, and OSTBC for 4×4 MIMO systems in i.i.d. Rayleigh fading channels. The crossover points are marked with circles, where D-V and V-O denote the crossover points for D-BLAST/V-BLAST and V-BLAST/OSTBC, respectively.

transmission. We evaluate the performances using the source coder SPIHT [34], for the 8 bits per pixel (bpp) 512×512 Lena image with a transmission rate of 0.5 bpp. The end-to-end performance is measured by the expected distortion of the image.

To begin, we summarize the evaluation of the expected distortion as stated in [12, Section V]: The system takes the compressed progressive bitstream and transforms it into a sequence of N_P packets with both error detection and error correction capability. Then, each coded packet is encoded by a space–time code. At the receiver, if a received packet is correctly decoded, the next packet is considered by the source decoder. Otherwise, the decoding is stopped, and the source is reconstructed from only the correctly decoded packets. We assume a slow-fading channel such that channel coefficients are nearly constant over an image, which consists of a sequence of N_P progressive packets. Let $P_i(\dot{\gamma}_{s,i})$ denote the conditional probability of a decoding error of the ith packet ($1 \le i \le N_P$) conditioned on $\dot{\gamma}_{s,i}$, the instantaneous SNR per symbol for the ith packet. Then, the probability that no decoding errors occur in the first n packets with an error in the next packet, i.e., $P_{c,n}$, is given by

$$P_{c,n} = P_{n+1}(\dot{\gamma}_{s,n+1}) \prod_{i=1}^{n} (1 - P_i(\dot{\gamma}_{s,i})) \text{ for } 1 \le n \le N_P - 1. \tag{53}$$

Note that $P_{c,0} = P_1(\dot{\gamma}_{s,1})$ is the probability of an error in the first packet, and $P_{c,N_P} = \prod_{i=1}^{N_P}(1 - P_i(\dot{\gamma}_{s,i}))$ is the probability that all N_P packets are correctly decoded. The distortion of the source when using the first n packets for the source decoder ($0 \le n \le N_P$) can be expressed as $D(\sum_{i=1}^{n} r_i)$, where r_i is the number of source bits in the ith packet, and $D(x)$ is the operational distortion-rate function of the source. Then, the expected distortion of the source, which is denoted by $E[D]$, can be expressed as (54), shown at the bottom of the next page, where $P_{c,n}$ is given by (53), and $p(\dot{\gamma}_{s,i})$ is the probability density function of the instantaneous SNR, i.e., $\dot{\gamma}_{s,i}$, for the ith packet. For $n = 0$, we have $D(\sum_{i=1}^{n} r_i) = D(0)$. From this, we have (53) and (54), and $E[D]$ can be rewritten as (55), shown at the bottom of the next page. Note that $p(\dot{\gamma}_{s,i})$ is a function of the average SNR per symbol, i.e., γ_s, as well as the spectral efficiency and the space–time code assigned to the ith packet; hence, $E[D]$ is also a function of those parameters. Note that $D(0)$ in (55) indicates the distortion for the event that there is an error in the first packet. For a still image, $D(0)$ means reconstructing the entire image at the mean pixel value; hence, the image is worthless. For a video, on the other hand, the decoder will hold over the previous frame for that frame. For low-motion videos, $D(0)$ might not be large.

Let C_i denote the space–time code assigned to the ith packet. One can find the optimal set of space–time codes $\mathbf{C}_{\text{opt}} = [C_1, \ldots, C_{N_P}]_{\text{opt}}$, which minimizes the expected distortion over a range of SNRs using the weighted cost function as follows:

$$\underset{C_1,\ldots,C_{N_P}}{\arg\min} \frac{\int_0^\infty \omega(\gamma_s) E[D] d\gamma_s}{\int_0^\infty \omega(\gamma_s) d\gamma_s} \tag{56}$$

where $w(\gamma_s) \in [0, 1]$ is the weight function. For example, $w(\gamma_s)$ can be chosen such that $w(\gamma_s) = 1$ for $\gamma_{s,a} \le \gamma_s \le \gamma_{s,b}$, and $w(\gamma_s) = 0$ otherwise. In broadcast or multicast systems, that weight function indicates that SNRs of multiple receivers are uniformly distributed in $\gamma_{s,a} \le \gamma_s \le \gamma_{s,b}$. Eq. (56) indicates that a set of space–time codes, i.e., $C_1, \ldots, C_{N_P}$, is chosen such that the total sum of the expected distortion of the receivers distributed in $\gamma_{s,a} \le \gamma_s \le \gamma_{s,b}$ is minimized. Note that the amount of computation involved in (56) exponentially grows as N_P increases. Alternatively, as presented in Section IV, we may choose a set of codes, i.e., $C_1, \ldots, C_{N_P}$, with the constraint that the earliest i consecutive packets should be encoded with OSTBC, the last j consecutive packets should be

encoded with V-BLAST, and the remaining $N_P - i - j$ packets are encoded with D-BLAST ($0 \le i, j \le N_P$ and $0 \le i+j \le N_P$).

To compare the image quality, we use the PSNR, defined as $10\log_{10}(255^2/E[D])$ (dB). We evaluate the PSNR performance as follows. We first compute (56) using the expected distortion, i.e., $E[D]$, given by (55), and the weight function, i.e., $w(\gamma_s)$, given below (56). Next, with the optimal set of codes, i.e., $\mathbf{C}_{\text{opt}} = [C_1, \ldots, C_{N_P}]_{\text{opt}}$, obtained from (56), we evaluate the PSNR over a range of SNRs, i.e., $\gamma_{s,a} \le \gamma_s \le \gamma_{s,b}$, given below (56). The performance is numerically evaluated for the case that a sequence of $N_P = 11$ progressive packets is transmitted in 2×2 MIMO systems as an example, and we assume that the spectral efficiencies are assigned in a way such that $\mathbf{R} = [2.0, 2.5, 3.0, 3.5, 4.0, 4.5, 5.0, 5.5, 6.0, 7.0, 8.0]$ (bits/s/Hz), where the ith component, i.e., R_i, is the spectral efficiency assigned to the ith packet. For this specific setup, the optimal set of space–time codes computed from (56) is given by $C_1 =$ OSTBC, $C_2 = C_3 = \cdots = C_9 =$ D-BLAST, and $C_{10} = C_{11} =$ V-BLAST. Fig. 9 shows the PSNR of such an optimal set of space–time codes, in addition to showing the PSNRs of other suboptimal sets of codes, such as the sets at the 75th and 50th percentiles among the sets of codes (note that the number of possible sets is 3^{N_P}), and the worst set of codes that shows the poorest performance. Fig. 9 also shows the PSNR corresponding to the expected distortion that is averaged over all the possible sets of space–time codes. From this example, it is seen that PSNR performance of the progressive source is sensitive to the way space–time codes are assigned to a sequence of packets, in part due to the unequal target error rates and spectral efficiencies of the bitstream.

Fig. 9 also shows the PSNR performance when (56) is computed with the constraint presented in Section IV. In this case, the number of possible sets of space–time codes is reduced to $\binom{N_P+1}{2}$. We note that the same optimal set of codes has been obtained when (56) is computed with and without the constraint. That is, without losing any PSNR performance, the computational complexity involved with the optimization can be reduced by exploiting the monotonic behavior of the crossover point, as shown in Fig. 2. It is further seen that the PSNR performance that corresponds to the expected distortion averaged over all possible sets of codes becomes better when the constraint in Section IV is introduced, which shows that, on average, the constraint in Section IV is a good strategy for the space–time coding of progressive sources. The simulation parameters involved in the evaluation of the PSNR performance are summarized in Table I.

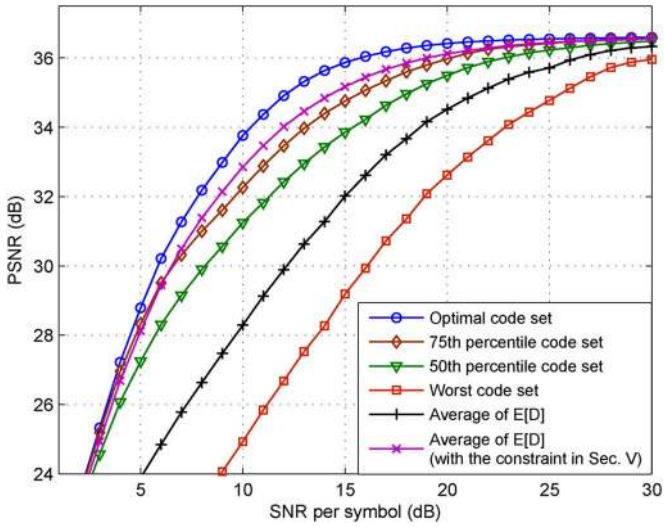

Fig. 9. PSNR performance of the optimal set of space–time codes and suboptimal space–time codes for the transmission of a progressive 8-bpp 512×512 Lena image for 2×2 MIMO systems in i.i.d. Rayleigh fading channels.

Fig. 10 shows the PSNR performance of the optimal set of space–time codes for 3×3 and 4×4 MIMO systems. Furthermore, it shows the performance of the optimal set of codes for the event that only V-BLAST and OSTBC are

$$E[D] = \int_0^\infty \cdots \int_0^\infty \left\{ \sum_{n=0}^{N_P} \left(D\left(\sum_{i=1}^{n} r_i \right) P_{c,n} \right) \right\} p(\dot{\gamma}_{s,1}) \cdots p(\dot{\gamma}_{s,N_P}) d\dot{\gamma}_{s,1} \cdots d\dot{\gamma}_{s,N_P}$$
$$= \int_0^\infty \cdots \int_0^\infty \left\{ D(0) P_{c,0} + \sum_{n=1}^{N_P-1} \left(D\left(\sum_{i=1}^{n} r_i \right) P_{c,n} \right) + D\left(\sum_{i=1}^{N_P} r_i \right) P_{c,N_P} \right\} p(\dot{\gamma}_{s,1}) \cdots p(\dot{\gamma}_{s,N_P}) d\dot{\gamma}_{s,1} \cdots d\dot{\gamma}_{s,N_P} \quad (54)$$

$$E[D] = \int_0^\infty \cdots \int_0^\infty \left\{ D(0) P_1(\dot{\gamma}_{s,1}) + \sum_{n=1}^{N_P-1} \left(D\left(\sum_{i=1}^{n} r_i \right) P_{n+1}(\dot{\gamma}_{s,n+1}) \prod_{i=1}^{n} (1 - P_i(\dot{\gamma}_{s,i})) \right) \right.$$
$$\left. + D\left(\sum_{i=1}^{N_P} r_i \right) \prod_{i=1}^{N_P} (1 - P_i(\dot{\gamma}_{s,i})) \right\} p(\dot{\gamma}_{s,1}) \cdots p(\dot{\gamma}_{s,N_P}) d\dot{\gamma}_{s,1} \cdots d\dot{\gamma}_{s,N_P} \quad (55)$$

TABLE I
SYSTEM PARAMETERS INVOLVED IN THE SIMULATION OF PSNR PERFORMANCE

	Fig. 9	Fig. 10	Fig. 13	Fig. 14
Image	Lena (8 bpp)	Lena (8 bpp)	Lena (8 bpp)	Pepper (8 bpp) Cameraman (8 bpp)
Resolution	512×512	512×512	512×512	512×512 256×256
Transmission rate	0.5 bpp	0.5 bpp	0.5 bpp	0.5 bpp
Number of antennas (Nt, Nr)	$N_t = N_r = 2$	$N_t = N_r = 3$ $N_t = N_r = 4$	$N_t = N_r = 2$	$N_t = N_r = 2$
Spatial correlation coefficients (ρ_t, ρ_r)	$\rho_t = \rho_r = 0.0$	$\rho_t = \rho_r = 0.0$	$\rho_t = \rho_r = 0.7$ $\rho_t = \rho_r = 0.0$	$\rho_t = \rho_r = 0.0$
Rician factor (K)	$K = 0.0$	$K = 0.0$	$K = 0.0$ $K = 2.0$	$K = 0.0$

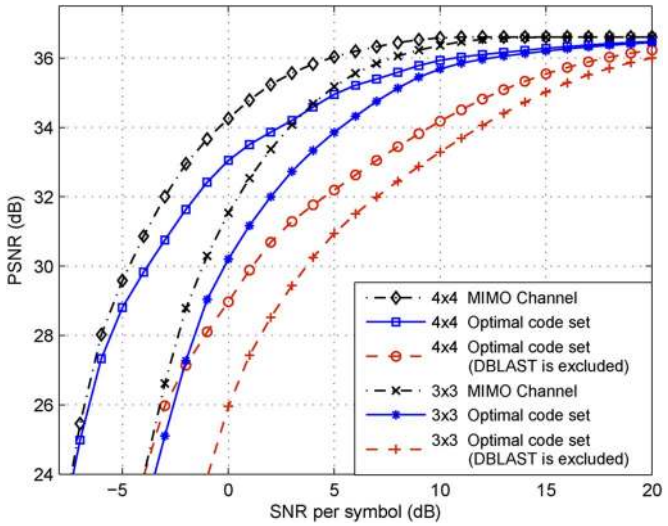

Fig. 10. PSNR performance of the optimal set of space–time codes for the transmission of a progressive 8-bpp 512×512 Lena image for 3×3 and 4×4 MIMO systems in i.i.d. Rayleigh fading channels. Dashed curves denote the performance of the optimal set of codes for the case when D-BLAST is excluded (i.e., only V-BLAST and OSTBC are used). Dash-dotted curves denote the performance for the case when the outage probabilities are calculated from the mutual information of MIMO channels.

employed (i.e., D-BLAST is excluded). For reference, Fig. 10 also shows the performance of the case where the outage probabilities are calculated from the mutual information of the MIMO channels [22]; that is, for the ith packet, the outage probability is obtained from

$$P_{\text{out}}(\gamma_s) = P\Big[\log\det\left(\mathbf{I}_{N_r} + \gamma_s \mathbf{H}\mathbf{H}^H\right) < R_i\Big] \qquad (57)$$

where R_i is the spectral efficiency assigned to that packet, and $\mathbf{I}_{N_r}$ denotes the $N_r \times N_r$ identity matrix. As can be seen in Fig. 10, there is a significant PSNR performance gap between the two cases where D-BLAST is excluded and not excluded.[2] This indicates that when progressive sources are transmitted in MIMO systems, the PSNR performance would improve if more space–time codes are considered for a sequence of packets. This motivated us to address the optimization strategy for a variety of space–time codes and their receivers rather than just V-BLAST with a zero-forcing receiver and OSTBC that were taken into account in our previous work [12]. Note that only three specific space–time codes, i.e., D-BLAST, V-BLAST, and OSTBC, are taken into account in Section III; however, the analysis in Section II can be exploited to optimize the progressive transmission that employs a variety of space–time codes and receivers with given DMT characteristic functions.

In the following, instead of the i.i.d. MIMO Rayleigh fading channels described in Section II, we also consider spatially correlated Rayleigh fading and Rician fading channels. Note that DMT characteristics, with multiplexing and diversity gains defined in (2) and (3) at high SNR, respectively, are not influenced by spatial correlation or line-of-sight (LOS) signal components [35], [36]. In other words, the DMT function for spatially correlated Rayleigh fading or Rician fading is identical to that for i.i.d. Rayleigh fading. This is because, as stated in [35], when the SNR approaches infinity, only the number of channel eigenmodes determines the performance, i.e., the relative strength of eigenmodes does not affect high-SNR behavior. Since spatial correlation or LOS components primarily affect the condition number of the channel matrix (i.e., the ratio of the maximum singular value to the minimum singular value), the impact of such propagation is not observed at high SNR. From this, it follows that the analysis of the crossover points presented in Section II is also valid over correlated Rayleigh fading or Rician fading channels at high SNR.

We numerically investigate the behavior of the crossover point in those propagation channels, which can be modeled as [37]

$$\mathbf{H}_c = \sqrt{\frac{K}{K+1}}\bar{\mathbf{H}} + \sqrt{\frac{1}{K+1}}\mathbf{R}_r^{1/2}\,\mathbf{H}\,\mathbf{R}_t^{1/2} \qquad (58)$$

where $K > 0$ is the Rician factor, and $\bar{\mathbf{H}}$ represents the average channel matrix related to LOS signal components. The Frobenius norm of $\bar{\mathbf{H}}$ is normalized as $(N_r N_t)^{1/2}$, and $\bar{\mathbf{H}}$ is assumed to be known to both the transmitter and the receiver. $\mathbf{R}_t$ is an $N_t \times N_t$ transmit spatial correlation matrix, $\mathbf{R}_r$ is an $N_r \times N_r$ receive spatial correlation matrix, $(\cdot)^{1/2}$ stands for the Hermitian square root of a matrix, and $\mathbf{H}$ is an $N_r \times N_t$ i.i.d. channel matrix, as defined in Section II. We use an exponential correlation model at the transmitter and the receiver with $(\mathbf{R}_t)_{i,j} = \rho_t^{|i-j|}$ and $(\mathbf{R}_r)_{i,j} = \rho_r^{|i-j|}$, where $(\cdot)_{i,j}$ denotes the (i,j)th element of a matrix, and ρ_t and ρ_r are the transmit and receive spatial correlation coefficients between

[2]Although not depicted here, the PSNR gap becomes even larger for more antennas, whereas the gap is not significant for 2×2 systems.

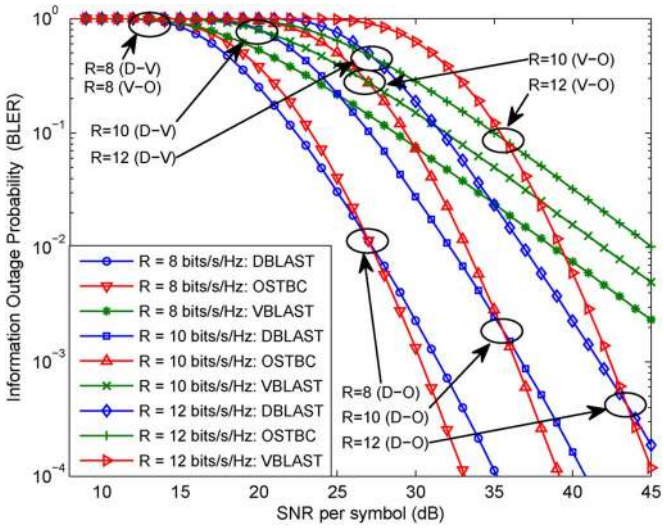

Fig. 11. Exact outage probabilities of D-BLAST, V-BLAST, and OSTBC for 2×2 MIMO systems in spatially correlated Rayleigh fading channels with $\rho_t = \rho_r = 0.7$. The crossover points are marked with circles, where D-O, D-V, and V-O denote the crossover points for D-BLAST/OSTBC, D-BLAST/V-BLAST, and V-BLAST/OSTBC, respectively.

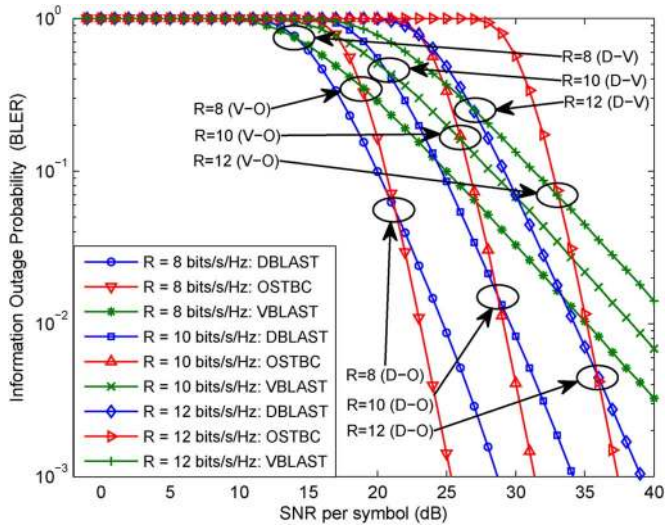

Fig. 12. Exact outage probabilities of D-BLAST, V-BLAST, and OSTBC for 2×2 MIMO systems in Rician fading channels with $K = 2$. The crossover points are marked with circles, where D-O, D-V, and V-O denote the crossover points for D-BLAST/OSTBC, D-BLAST/V-BLAST, and V-BLAST/OSTBC, respectively.

adjacent antennas, respectively. The exact outage probabilities are numerically evaluated, as an example, for 2×2 spatially correlated Rayleigh fading channels with various correlation coefficients. The results for $\rho_t = \rho_r = 0.7$ are shown in Fig. 11. It is seen that the crossover points in the correlated Rayleigh fading channels behave in the same way as those for the i.i.d. Rayleigh fading channels do. Next, the exact outage probabilities are evaluated for 2×2 Rician fading channels, and the results for a Rician factor of $K = 2$ are shown in Fig. 12. It is also seen that the crossover points exhibit the same behavior as those for the i.i.d. Rayleigh fading channels.[3]

Fig. 13 shows the PSNR performance for spatially correlated Rayleigh fading channels with $\rho_t = \rho_r = 0.7$, and Rician fading channels with $K = 2$, where the other system parameters are the same as those for i.i.d. Rayleigh fading channels, whose results are shown in Fig. 9. Note that, for each propagation channel, the same optimal set of space–time codes has been obtained when (56) is computed with and without the constraint. Furthermore, similar to the results for i.i.d. Rayleigh fading, the PSNR performance, which corresponds to the expected distortion averaged over all the possible sets of space–time codes, becomes better when the constraint in Section IV is introduced. This indicates that, even for spatially correlated Rayleigh fading or Rician fading channels, the constraint in Section IV is a good optimization strategy for the space–time coding of progressive sources.

In Fig. 14, we observe the performance for other images, such as 8-bpp 512×512 Pepper and 256×256 Cameraman, each with a rate of 0.5 bpp, in i.i.d. Rayleigh fading channels. In Fig. 14, for either Pepper or Cameraman, the same optimal set of space–time codes has been obtained when (56) is evaluated

[3]For other spatial correlation coefficients and Rician factors, the corresponding crossover points show the same behavior; thus, they are not depicted here.

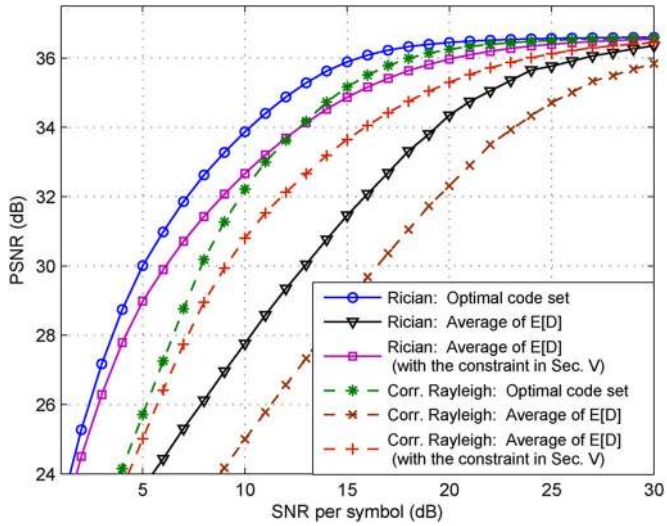

Fig. 13. PSNR performance for the transmission of a progressive 8-bpp 512×512 Lena image for 2×2 MIMO systems in spatially correlated Rayleigh fading channels with $\rho_t = \rho_r = 0.7$ and Rician fading channels with $K = 2$.

either with or without the constraint in Section IV, similar to the results for the Lena image, as shown in Fig. 9.

Finally, we note that our analysis in Sections III and IV can also be applied to scalable video, in addition to progressive images. In scalable video, the base layer is more important than the enhancement layer. If the base layer is split into multiple packets, those packets often have a similar level of importance. However, the enhancement layer (for example, with medium-grain scalability) can usually be split into multiple packets with successively decreasing importance. Hence, for real-time scalable video, we can apply our analytical results to the sequence of high-importance base-layer packets and successively less important enhancement-layer packets.

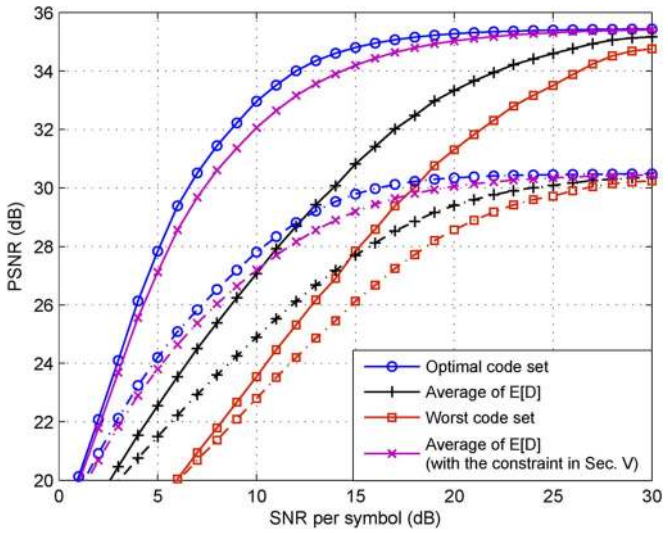

Fig. 14. PSNR performance for the transmission of a progressive 8-bpp 512×512 Pepper image (solid curves) and 256×256 Cameraman image (dash-dotted curves) for 2×2 MIMO systems in i.i.d. Rayleigh fading channels.

VI. Conclusion

When we transmit a sequence of multimedia progressive packets over MIMO channels, due to the differences in importance in the bitstream, the tradeoff between the space–time codes, which are under consideration to encode each packet, should be clarified in terms of their target error rates and spectral efficiencies. By exploiting DMT functions, we analyzed the crossover point of the outage probability curves of the space–time codes. The results showed that as long as the crossover point of the outage probabilities exists, as the spectral efficiency increases, the crossover point in the SNR monotonically increases, whereas that in outage probability monotonically decreases. The work in this paper extended [12] to more general cases, in that the given results can be applied to any space–time codes, receivers, and propagation channels with given DMT functions.

As a specific example, we took D-BLAST with a group zero-forcing receiver, V-BLAST with an MMSE receiver, and OSTBC into account and showed the monotonic behavior of the crossover points, which holds in spatially correlated Rayleigh and Rician fading channels, as well as in i.i.d. Rayleigh fading channels. Based on that, we derived the optimization method with respect to D-BLAST, V-BLAST, and OSTBC for the space–time coding of a sequence of numerous progressive packets.

The numerical evaluation showed that the PSNR performance improves (nearly by 2 dB at the PSNR of 34 dB) when D-BLAST is introduced, in addition to V-BLAST and OSTBC. This motivated us to address the optimization strategy for a variety of space–time codes, rather than just that for V-BLAST and OSTBC that were considered in [12]. The evaluation showed that, without any PSNR degradation, the computational complexity involved with optimal space–time coding is exponentially reduced by the use of the derived optimization method. Furthermore, it was shown that the PSNR performance averaged over all the possible sets of space–time codes becomes better when the derived optimization method is used, which indicates that, on average, it is a good strategy for the space–time coding of multimedia progressive sources.

Our analysis allows a tradeoff between space–time codes in terms of their target error rates and transmission data rates (i.e., spectral efficiencies), from which the optimization strategy for the progressive transmission can be derived. The work in this paper has significance in terms of its impact on multimedia communications and its analysis for the monotonic behavior of the crossover points, which deepens our understanding of the tradeoff between space–time codes.

Appendix A
Proof of the Analysis in Section III-A

i) $0 < r \leq 2/(N_t+1)$: From (44) and (45), it is seen that the condition of (38) is satisfied when we set $d_1(r) = d_V(r)$ and $d_2(r) = d_D(r)$ in (15). Furthermore, from $N_r \geq N_t \geq 2$, it can be shown that

$$d_D(0) - d_V(0) = N_r(N_t - 1) > 0 \tag{59}$$

$$d_D(2/(N_t+1)) - d_V(2/(N_t+1)) = \frac{(N_r(N_t^2-2)-2)(N_t-1)}{N_t(N_t+1)} > 0. \tag{60}$$

Eqs. (59) and (60) satisfy the conditions of (39) and (40), respectively, when we set $\alpha = \varepsilon$ and $\beta = 2/(N_t+1)$, where $\varepsilon > 0$ denotes an arbitrarily small positive number. Hence, the result in Section II-D, which is given by (41), holds for $(2^R/k_r)^{(N_t+1)/2} \leq \gamma_s < \infty$.

ii) $2/(N_t+1) \leq r \leq 2N_t/(N_t+1)$: We set $d_1(r) = d_V(r)$ and $d_2(r) = d_D(r)$ in (15). Then, from (44) and (45), the condition of (16) is satisfied. From $N_r \geq N_t \geq 2$, it can be shown that

$$d_D(2N_t/(N_t+1)) - d_V(2N_t/(N_t+1)) = -\frac{(N_r - N_t + 1)(N_t - 1)}{(N_t+1)} < 0. \tag{61}$$

Setting $\alpha = 2/(N_t+1)$ and $\beta = 2N_t/(N_t+1)$, (60) and (61) satisfy the conditions of (17) and (18), respectively, so that the result in Section II-A, which is given by (24) and (25), holds for $(2^R/k_r)^{(N_t+1)/2N_t} \leq \gamma_s \leq (2^R/k_r)^{(N_t+1)/2}$.

iii) $2N_t/(N_t+1) \leq r \leq N_t$: We set $d_1(r) = d_D(r)$ and $d_2(r) = d_V(r)$ in (15). Then, (33) is met from (44) and (45). Furthermore, we have

$$d_D(N_t) = d_V(N_t) = 0. \tag{62}$$

Eqs. (61) and (62) satisfy the conditions of (34) and (35), respectively, when setting $\alpha = 2N_t/(N_t+1)$ and $\beta = N_t$; thus, the result in Section II-C, which is given by (37), holds for $(2^R/k_r)^{1/N_t} \leq \gamma_s \leq (2^R/k_r)^{(N_t+1)/2N_t}$.

iv) $N_t \le r < \infty$: For this range, from (44) and (45), we have $d_D(r) = d_V(r) = 0$. Since the two DMT functions coincide, the result in Section II-E, which is given by (43), holds for $1 < \gamma_s \le (2^R/k_r)^{1/N_t}$.

APPENDIX B
PROOF OF THE ANALYSIS IN SECTION III-B

Cases 1 and 2: $N_r \ge N_t \ge 3$, or $N_t = 2$ and $N_r \ge 4$

i) $0 < r \le 2/(N_t+1)$: From (44) and (46), the condition of (16) is met, as we set $d_1(r) = d_D(r)$ and $d_2(r) = d_O(r)$ in (15). In addition, it can be shown that

$$d_D(0) - d_O(0) = 1 - N_t < 0 \tag{63}$$

$$d_D(2/(N_t+1)) - d_O(2/(N_t+1)) = \frac{-r_s N_t^2 + (2-r_s)N_r N_t + r_s(1-N_r)}{r_s(N_t+1)} > 0. \tag{64}$$

The inequality in (64) is proven in the following: Let $f(N_t) = -r_s N_t^2 + (2-r_s)N_r N_t + r_s(1-N_r)$ be the numerator of (64). We will show that $f(N_t) > 0$ for either $N_r \ge N_t \ge 3$, or $N_t = 2$ and $N_r \ge 4$.

a) We first consider the case of $N_t \ge 5$: It can be shown that $f(N_t)$ is a monotonically increasing function in N_t for $N_t \le N_r(2-r_s)/2r_s$. From $r_s = 1/2$, we have $(2-r_s)N_r/2r_s = 3N_r/2$. From this and $N_r \ge N_t \ge 5$, it follows that $f(N_t) \ge f(5) = 7N_r - 12 > 0$.
b) Next, we consider the case of $N_t = 3$ or 4: From $r_s = 3/4$ and $N_r \ge N_t$, we have $f(3) = 3N_r - 6 > 0$ and $f(4) = (17N_r - 45)/4 > 0$.
c) Finally, we consider the case of $N_t = 2$ and $N_r \ge 4$: From $r_s = 1$ and $N_r \ge 4$, we have $f(2) = N_r - 3 > 0$.

Eqs. (63) and (64) satisfy the conditions of (17) and (18), respectively, when setting $\alpha = \varepsilon$ and $\beta = 2/(N_t+1)$. Thus, the result in Section II-A, which is given by (24) and (25), holds for $(2^R/k_r)^{(N_t+1)/2} \le \gamma_s < \infty$.

ii) $2/(N_t+1) \le r \le r_s$: We set $d_1(r) = d_O(r)$ and $d_2(r) = d_D(r)$ in (15). Then, (38) is satisfied from (44) and (46). From $N_t \ge 2$ and $r_s \le 1$, it can be readily shown that

$$d_D(r_s) - d_O(r_s) = (N_r - 1)(N_t - r_s(N_t+1)/2) > 0. \tag{65}$$

Eqs. (64) and (65) meet the conditions of (39) and (40), respectively, by setting $\alpha = 2/(N_t+1)$ and $\beta = r_s$; thus, the result in Section II-D, which is given by (41), holds for $(2^R/k_r)^{1/r_s} \le \gamma_s \le (2^R/k_r)^{(N_t+1)/2}$.

iii) $r_s \le r \le 2N_t/(N_t+1)$: We set $d_1(r) = d_O(r)$ and $d_2(r) = d_D(r)$ in (15). Then, from (44) and (46), the condition of (33) is met. In addition, we have

$$d_D(2N_t/(N_t+1)) = d_O(2N_t/(N_t+1)) = 0. \tag{66}$$

Setting $\alpha = r_s$ and $\beta = 2N_t/(N_t+1)$, (65) and (66) meet the conditions of (34) and (35), respectively. Thus, the result in Section II-C, which is given by (37), holds for $(2^R/k_r)^{(N_t+1)/2N_t} \le \gamma_s \le (2^R/k_r)^{1/r_s}$.

iv) $2N_t/(N_t+1) \le r < \infty$: For this range, from (44) and (46), we have $d_D(0) = d_O(r) = 0$. The result in Section II-E, which is given by (43), holds for $1 < \gamma_s \le (2^R/k_r)^{(N_t+1)/2N_t}$.

Case 3: $N_t = 2$ and $N_r = 3$

i) $0 < r \le 2/(N_t+1)$: We set $d_1(r) = d_D(r)$ and $d_2(r) = d_O(r)$ in (15). Then, (33) is satisfied from (44) and (46). From $N_t = 2$, $N_r = 3$, and $r_s = 1$, (64) is modified into

$$d_D(2/(N_t+1)) - d_O(2/(N_t+1)) = 0. \tag{67}$$

Eqs. (63) and (37) meet the conditions of (34) and (35), respectively. Hence, the result in Section II-C, which is given by (37), holds for $(2^R/k_r)^{(N_t+1)/2} \le \gamma_s < \infty$.

ii) $2/(N_t+1) \le r \le 1$: We set $d_1(r) = d_O(r)$ and $d_2(r) = d_D(r)$ in (15). Then, from (44) and (46), the condition of (26) is satisfied. Moreover, (67) and (65) meet the conditions of (27) and (28), respectively, so that the result in Section II-B, which is given by (31) and (42), holds for $2^R/k_r \le \gamma_s \le (2^R/k_r)^{(N_t+1)/2}$.

Case 4: $N_t = N_r = 2$

i) $0 < r \le 2/(N_t+1)$: We set $d_1(r) = d_D(r)$ and $d_2(r) = d_O(r)$ in (15). Then, from (44) and (46), the condition of (38) is met. From $N_t = N_r = 2$ and $r_s = 1$, (64) is changed into

$$d_D(2/(N_t+1)) - d_O(2/(N_t+1)) < 0. \tag{68}$$

Eqs. (63) and (68) satisfy the conditions of (39) and (40), respectively; thus, the result in Section II-D, which is given by (41), holds for $(2^R/k_r)^{(N_t+1)/2} \le \gamma_s < \infty$.

ii) $2/(N_t+1) \le r \le 1$: We set $d_1(r) = d_D(r)$ and $d_2(r) = d_O(r)$ in (15). Then, (16) is satisfied from (44) and (46). Furthermore, (68) and (65) meet the conditions of (17) and (18), respectively, so that the result in Section II-A, which is given by (24) and (25), holds for $2^R/k_r \le \gamma_s \le (2^R/k_r)^{(N_t+1)/2}$.

REFERENCES

[1] H. Zhang, Y. Zheng, M. A. Khojastepour, and S. Rangarajan, "Cross-layer optimization for streaming scalable video over fading wireless networks," *IEEE J. Select. Areas Commun.*, vol. 28, no. 3, pp. 344–353, Apr. 2010.

[2] Z. Yang and X. Wang, "Scalable video broadcast over downlink MIMO-OFDM systems," *IEEE Trans. Circuits Syst. Video Technol.*, vol. 23, no. 2, pp. 212–223, Feb. 2013.

[3] S.-H. Chang, "*Joint Optimization of Physical and Application Layers for Wireless Multimedia Communications*," Ph.D. dissertation, Univ. California, San Diego, CA, USA, 2010.

[4] Y. Jin and H.-J. Lee, "A block-based pass-parallel SPIHT algorithm," *IEEE Trans. Circuits Syst. Video Technol.*, vol. 22, no. 7, pp. 1064–1075, Jul. 2012.

[5] D. Taubman and M. Marcellin, *JPEG2000: Image Compression Fundamentals, Standards, and Practice*. Norwell, MA, USA: Kluwer, 2001.

[6] H. Schwarz, D. Marpe, and T. Wiegand, "Overview of the scalable video coding extension of H.264/AVC," *IEEE Trans. Circuits Syst. Video Technol.*, vol. 17, no. 9, pp. 1103–1120, Sep. 2007.

[7] J. Reichel, H. Schwarz, and M. Wien, Eds., "Scalable Video Coding—Working Draft 1," Joint Video Team of ITU-T VCEG and ISO/IEC MPEG, Doc. JVT-N020, Hong Kong, Jan. 2005.

[8] G. J. Foschini and M. J. Gans, "On limits of wireless communications in a fading environment when using multiple antennas," *Wireless Pers. Commun.*, vol. 6, no. 3, pp. 311–335, Mar. 1998.

[9] R. Louie, M. McKay, and I. Collings, "Open-loop spatial multiplexing and diversity communications in ad hoc networks," *IEEE Trans. Inf. Theory*, vol. 57, no. 1, pp. 317–344, Jan. 2011.
[10] V. Tarokh, H. Jafarkhani, and A. R. Calderbank, "Space–time block codes from orthogonal designs," *IEEE Trans. Inf. Theory*, vol. 45, no. 5, pp. 1456–1467, Jul. 1999.
[11] A. Lozano and N. Jindal, "Transmit diversity vs. spatial multiplexing in modern MIMO systems," *IEEE Trans. Wireless Commun.*, vol. 9, no. 1, pp. 186–197, Jan. 2010.
[12] S.-H. Chang, P. C. Cosman, and L. B. Milstein, "Optimal transmission of progressive sources based on the error probability analysis of SM and OSTBC," *IEEE Trans. Veh. Technol.*, vol. 63, no. 1, pp. 94–106, Jan. 2014.
[13] L. Zheng and D. N. C. Tse, "Diversity and multiplexing: A fundamental tradeoff in multiple-antenna channels," *IEEE Trans. Inf. Theory*, vol. 49, no. 5, pp. 1073–1096, May 2003.
[14] Y. Lu, W. Zhang, and X.-G. Xia, "On diversity and multiplexing tradeoff of two-layer D-BLAST with group zero-forcing detection," *IEEE Trans. Commun.*, vol. 60, no. 8, pp. 2255–2264, Aug. 2012.
[15] B. Hassibi and B. Hochwald, "High-rate codes that are linear in space and time," *IEEE Trans. Inf. Theory*, vol. 48, no. 7, pp. 1804–1824, Jul. 2002.
[16] R. W. Heath, Jr., and A. J. Paulraj, "Linear dispersion codes for MIMO systems based on frame theory," *IEEE Trans. Signal Process.*, vol. 50, no. 10, pp. 2429–2441, Oct. 2002.
[17] J.-C. Belfiore, G. Rekaya, and E. Viterbo, "The Golden code: A 2×2 full-rate space–time code with non-vanishing determinants," *IEEE Trans. Inf. Theory*, vol. 51, no. 4, pp. 1432–1436, Apr. 2005.
[18] F. Oggier, G. Rekaya, J.-C. Belfiore, and E. Viterbo, "Perfect space–time block codes," *IEEE Trans. Inf. Theory*, vol. 52, no. 9, pp. 3885–3902, Sep. 2006.
[19] P. Elia, K. R. Kumar, S. A. Pawar, P. V. Kumar, and H.-F. Lu, "Explicit, minimum-delay space–time codes achieving the diversity–multiplexing gain tradeoff," *IEEE Trans. Inf. Theory*, vol. 52, no. 9, pp. 3869–3884, Sep. 2006.
[20] B. A. Sethuraman, B. S. Rajan, and V. Shashidhar, "Full-diversity, high-rate space–time block codes from division algebras," *IEEE Trans. Inf. Theory*, vol. 49, no. 10, pp. 2596–2616, Oct. 2003.
[21] C. Oestges and B. Clerckx, *MIMO Wireless Communications*. Orlando, FL, USA: Academic, 2007.
[22] K. Raj Kumar, G. Caire, and A. L. Moustakas, "Asymptotic performance of linear receivers in MIMO fading channels," *IEEE Trans. Inf. Theory*, vol. 55, no. 10, pp. 4398–4418, Oct. 2009.
[23] X. Guo and X.-G. Xia, "On full diversity space–time block codes with partial interference cancellation group decoding," *IEEE Trans. Inf. Theory*, vol. 55, no. 10, pp. 4366–4385, Oct. 2009.
[24] N. Prasad and X. Wang, "Outage minimization and rate allocation for the multiuser Gaussian interference channels with successive group decoding," *IEEE Trans. Inf. Theory*, vol. 55, no. 12, pp. 5540–5557, Nov. 2009.
[25] W. Zhang, T. Xu, and Z.-G. Xia, "Two designs of space–time block codes achieving full diversity with partial interference cancellation group decoding," *IEEE Trans. Inf. Theory*, vol. 58, no. 2, pp. 747–764, Feb. 2012.
[26] L. Shi, W. Zhang, and Z.-G. Xia, "High-rate and full-diversity space–time block codes with low complexity partial interference cancellation group decoding," *IEEE Trans. Commun.*, vol. 59, no. 5, pp. 1201–1207, May 2011.
[27] T. Xu and X.-G. Xia, "On space–time code design with a conditional PIC group decoding," *IEEE Trans. Inf. Theory*, vol. 57, no. 6, pp. 3582–3593, Jun. 2011.
[28] C. Gong, A. Tajer, and X. Wang, "Interference channel with constrained partial group decoding," *IEEE Trans. Inf. Theory*, vol. 59, no. 11, pp. 3059–3071, Nov. 2011.
[29] D. Tse and P. Viswanath, *Fundamentals of Wireless Communication*. New York, NY, USA: Cambridge Univ. Press, 2005.
[30] O. Tirkkonen and A. Hottinen, "Square-matrix embeddable space–time block codes for complex signal constellations," *IEEE Trans. Inf. Theory*, vol. 48, no. 2, pp. 384–395, Feb. 2002.
[31] L. Toni, Y. S. Chan, P. C. Cosman, and L. B. Milstein, "Channel coding for progressive images in a 2-D time–frequency OFDM block with channel estimation errors," *IEEE Trans. Image Process.*, vol. 18, no. 11, pp. 2476–2490, Nov. 2009.
[32] V. Stankovic, R. Hamzaoui, Y. Charfi, and Z. Xiong, "Real-time unequal error protection algorithms for progressive image transmission," *IEEE J. Sel. Areas Commun.*, vol. 21, no. 10, pp. 1526–1535, Dec. 2003.
[33] S.-H. Chang, P. C. Cosman, and L. B. Milstein, "Iterative channel decoding of FEC-based multiple description codes," *IEEE Trans. Image Process.*, vol. 21, no. 3, pp. 1138–1152, Mar. 2012.
[34] A. Said and W. A. Pearlman, "A new, fast, and efficient image codec based on set partitioning in hierarchical trees," *IEEE Trans. Circuits Syst. Video Technol.*, vol. 6, no. 3, pp. 243–249, Jun. 1996.
[35] R. Narasimhan, "Finite-SNR diversity–multiplexing tradeoff for correlated Rayleigh and Rician MIMO channels," *IEEE Trans. Inf. Theory*, vol. 52, no. 9, pp. 3965–3979, Sep. 2006.
[36] L. Zhao, W. Mo, Y. Ma, and Z. Wang, "Diversity and multiplexing tradeoff in general fading channels," *IEEE Trans. Inf. Theory*, vol. 53, no. 4, pp. 1549–1557, Apr. 2007.
[37] G. Taricco and E. Riegler, "On the ergodic capacity of correlated Rician fading MIMO channels with interference," *IEEE Trans. Inf. Theory*, vol. 57, no. 7, pp. 4123–4137, Jul. 2011.

Seok-Ho Chang (S'07–M'10) received the B.S. and M.S. degrees from Seoul National University, Seoul, Korea, in 1997 and 1999, respectively, and the Ph.D. degree from the University of California, San Diego, CA, USA, in 2010, all in electrical engineering.

From 1999 to 2005, he was with LG Electronics, Korea, where he was involved in the development of WCDMA (3GPP) base/mobile-station modem chips. In 2006, he was with POSCO ICT, Korea, where he worked on mobile WiMax systems. From 2010 to 2011, he was a Postdoctoral Scholar with the University of California, San Diego, CA, USA, where he was engaged in the cross-layer design of wireless systems. From 2011 to 2012, he was a Staff Engineer with Qualcomm Inc., San Diego, CA, USA, where he was involved in the design and development of 4G cellular modem chips. Since September 2012, he has been an Assistant Professor with the Department of Computer Science and Engineering, Dankook University, Yongin, Korea. His research interests include wireless/wireline digital communication theory, signal processing, multiuser information theory, time and frequency synchronization, equalization, multiple-input–multiple-output systems, and cross-layer design of wireless systems.

Jihwan P. Choi (S'01–M'06) received the B.S. degree from Seoul National University, Seoul, Korea, in 1998, and both the S.M. and Ph.D. degrees in EECS from Massachusetts Institute of Technology (MIT), Cambridge, MA, USA, in 2000 and 2006, respectively.

From 1999 to 2006, he participated in the Next Generation Internet (NGI) satellite network project at MIT. From 2006 to 2012, he was with the Wireless R&D Group, Marvell Semiconductor Inc., Santa Clara, CA, USA, for mobile system design and standardization of 3G/4G commercial wireless communications including WiMAX and 3GPP LTE as Principal System Engineer. He is now an assistant professor with the Department of Information and Communication Engineering, Daegu Gyeongbuk Institute of Science & Technology (DGIST), Daegu, Korea. His research interests are in cross-layer system design for space/wireless networks.

Pamela C. Cosman (S'88–M'93–SM'00–F'08) received the B.S. degree with Honor in electrical engineering from the California Institute of Technology, Pasadena, CA, USA, in 1987 and the Ph.D. in electrical engineering from Stanford University, Stanford, CA, in 1993.

She was an NSF postdoctoral fellow at Stanford University and a Visiting Professor at the University of Minnesota during 1993–1995. In 1995, she joined the faculty of the department of Electrical and Computer Engineering at the University of California, San Diego, where she is currently a Professor, as well as Associate Dean for Students of the Jacobs School of Engineering. She was the Director of the Center for Wireless Communications from 2006 to 2008. Her research interests are in the areas of image and video compression and processing, and wireless communications.

Dr. Cosman's awards include the ECE Departmental Graduate Teaching Award, a Career Award from the National Science Foundation, a Powell Faculty Fellowship, Globecom 2008 Best Paper Award, and HISB 2012 Best Poster Award. She was a Guest Editor of the June 2000 special issue of the IEEE JOURNAL OF SELECTED AREAS IN COMMUNICATIONS "Error-resilient image and video coding" and was the Technical Program Chair of the 1998 Information Theory Workshop in San Diego. She has been a Member of the Technical Program Committee or the Organizing Committee for numerous conferences, including ICIP 2008–2011, QOMEX 2010–2012, ICME 2011–2013, VCIP 2010, Packet Video 2007–2013, WPMC 2006, ICISP 2003, ACIVS 2002–2012, ICC 2012, Asilomar Conference on Signals, Systems and Computers 2003, and EUSIPCO 1998. She was an Associate Editor of the IEEE COMMUNICATIONS LETTERS (1998–2001) and an Associate Editor of the IEEE SIGNAL PROCESING LETTERS (2001–2005). She was the Editor-in-Chief (2006–2009), as well as a Senior Editor (2003–2005, 2010–2013), of the IEEE JOURNAL ON SELECTED AREAS IN COMMUNICATIONS. She is a member of Tau Beta Pi and Sigma Xi.

Laurence B. Milstein (S'66–M'68–SM'77–F'85) received the B.E.E. degree from the City College of New York, New York, NY, USA, in 1964 and the M.S. and Ph.D. degrees in electrical engineering from the Polytechnic Institute of Brooklyn, Brooklyn, NY, in 1966 and 1968, respectively.

From 1968 to 1974, he was with the Space and Communications Group, Hughes Aircraft Company, and from 1974 to 1976, he was a member of the Department of Electrical and Systems Engineering, Rensselaer Polytechnic Institute, Troy, NY. Since 1976, he has been with the Department of Electrical and Computer Engineering, University of California, San Diego, La Jolla, CA, USA, where he is the Ericsson Professor of wireless communications access techniques and a former Department Chairman, working in the area of digital communication theory, with special emphasis on spread-spectrum communication systems. He has also been a consultant to both government and industry in the areas of radar and communications.

Dr. Milstein was an Associate Editor of Communication Theory for the IEEE TRANSACTIONS ON COMMUNICATIONS, an Associate Editor for Book Reviews for the IEEE TRANSACTIONS ON INFORMATION THEORY, an Associate Technical Editor for the IEEE COMMUNICATIONS MAGAZINE, and the Editor-in-Chief of the IEEE JOURNAL ON SELECTED AREAS IN COMMUNICATIONS. He was the Vice President for Technical Affairs in 1990 and 1991 of the IEEE Communications Society and is a former Chair of the IEEE Fellows Selection Committee. He received the 1998 Military Communications Conference Long-Term Technical Achievement Award, an Academic Senate 1999 UCSD Distinguished Teaching Award, an IEEE Third Millennium Medal in 2000, the 2000 IEEE Communication Society Armstrong Technical Achievement Award, and various prize paper awards, including the 2002 MILCOM Fred Ellersick Award.